Article

Cell Reports

Phospholipase D1 Ablation Disrupts Mouse Longitudinal Hippocampal Axis Organization and Functioning

Graphical Abstract

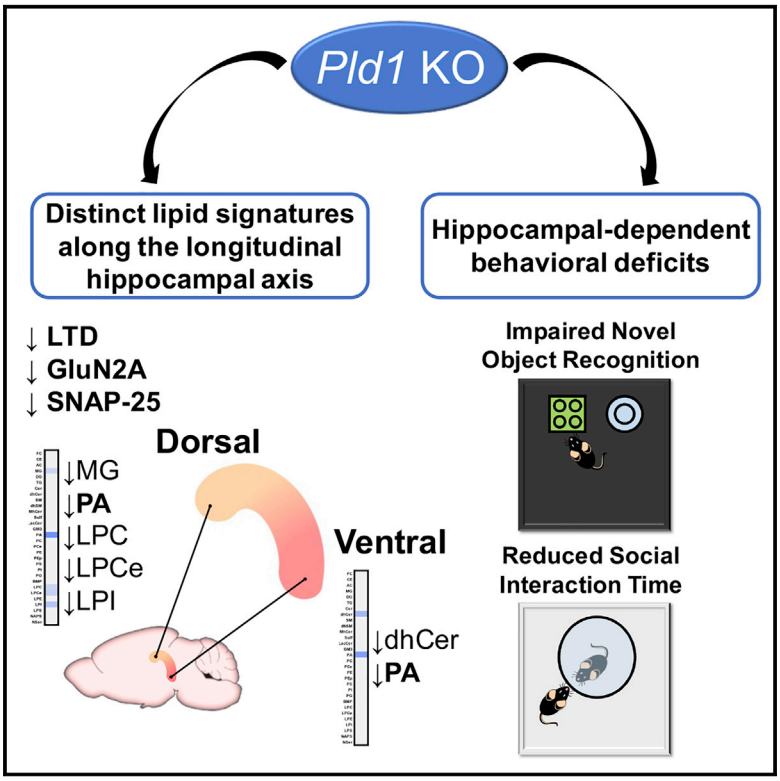

Highlights

- PLD1 is a major phosphatidic acid source compared to PLD2
- PLD1 KO mice show deficits in object recognition and social exploration
- PLD1 ablation disrupts DH-VH dendritic arborization differentiation
- PLD1 ablation reduces LTD induction and GluN2A and SNAP-25 levels in the DH

Authors

Luísa Santa-Marinha, Isabel Castanho, Rita Ribeiro Silva, ..., Gilbert Di Paolo, Vítor Pinto, Tiago Gil Oliveira

Correspondence

tiago@med.uminho.pt

In Brief

Santa-Marinha et al. show that PLD1 and PLD2 contribute differentially to the mouse hippocampal lipidomic profile. Their data highlight PLD1-derived PA reduction as a major modulator of dorsal-ventral hippocampal organization and functioning.

Santa-Marinha et al., 2020, Cell Reports *30*, 4197–4208
March 24, 2020
https://doi.org/10.1016/j.celrep.2020.02.102

CellPress

Cell Reports
Article

Phospholipase D1 Ablation Disrupts Mouse Longitudinal Hippocampal Axis Organization and Functioning

Luísa Santa-Marinha,[1,2,6] Isabel Castanho,[1,2,6,7] Rita Ribeiro Silva,[1,2] Francisca Vaz Bravo,[1,2] André Miguel Miranda,[1,2] Torcato Meira,[1,2] Rafaela Morais-Ribeiro,[1,2] Fernanda Marques,[1,2] Yimeng Xu,[3] Kimberly Point du Jour,[3,4,8] Markus Wenk,[5] Robin Barry Chan,[3,4] Gilbert Di Paolo,[3,4,9] Vítor Pinto,[1,2] and Tiago Gil Oliveira[1,2,10,*]

[1]Life and Health Sciences Research Institute (ICVS), School of Medicine, University of Minho, Campus Gualtar, 4710-057 Braga, Portugal
[2]ICVS/3B's - PT Government Associate Laboratory, Braga/Guimarães, Portugal
[3]Department of Pathology and Cell Biology, Columbia University Medical Center, New York, NY 10032, USA
[4]Taub Institute for Research on Alzheimer's Disease and the Aging Brain, Columbia University Medical Center, New York, NY 10032, USA
[5]Department of Biochemistry, Yong Loo Lin School of Medicine, National University of Singapore, Singapore 117596, Singapore
[6]These authors contributed equally
[7]Present address: Institute of Biomedical and Clinical Sciences, University of Exeter Medical School, University of Exeter, Exeter EX2 5DW, UK
[8]Present address: Emory University School of Medicine, Atlanta, GA 30308, USA
[9]Present address: Denali Therapeutics, South San Francisco, CA 94080, USA
[10]Lead Contact
*Correspondence: tiago@med.uminho.pt
https://doi.org/10.1016/j.celrep.2020.02.102

SUMMARY

Phosphatidic acid (PA) is a signaling lipid involved in the modulation of synaptic structure and functioning. Based on previous work showing a decreasing PA gradient along the longitudinal axis of the rodent hippocampus, we asked whether the dorsal hippocampus (DH) and the ventral hippocampus (VH) are differentially affected by PA modulation. Here, we show that phospholipase D1 (PLD1) is a major hippocampal PA source, compared to PLD2, and that PLD1 ablation affects predominantly the lipidome of the DH. Moreover, *Pld1* knockout (KO) mice show specific deficits in novel object recognition and social interaction and disruption in the DH-VH dendritic arborization differentiation in CA1/CA3 pyramidal neurons. Also, *Pld1* KO animals present reduced long-term depression (LTD) induction and reduced GluN2A and SNAP-25 protein levels in the DH. Overall, we observe that PLD1-derived PA reduction leads to differential lipid signatures along the longitudinal hippocampal axis, predominantly affecting DH organization and functioning.

INTRODUCTION

The hippocampus is a brain temporal lobe structure that is fundamental for learning and memory. Despite maintaining its cross-sectional architecture along its longitudinal axis, anatomical, gene expression, and functional studies overall suggest an organized gradient that segregates in the rodent dorsal hippocampus (DH) and ventral hippocampus (VH) poles, which correspond in primates to posterior and anterior poles (Strange et al., 2014). While a classical dichotomic view mainly implicated the DH in spatial navigation and episodic memory and the VH in affective and stress-related behaviors (Bannerman et al., 2014; Fanselow and Dong, 2010; Kheirbek et al., 2013; McHugh et al., 2011; Strange et al., 2014), addressing the differential functional roles of DH and VH should take into account a gradual biochemical and functional transition between the hippocampal poles (Bienkowski et al., 2018; Maggio and Segal, 2007; Miranda et al., 2019; Pinto et al., 2015; Shah et al., 2017; Thompson et al., 2008).

The development of tools such as mass spectrometry (MS) and the genetic modulation of lipid pathways has expanded the knowledge of the role of lipids in brain physiology and pathology (Chan et al., 2012; Miranda et al., 2019; Oliveira et al., 2016). Recently, the DH and VH were shown to differ in their sphingolipid and glycerophospholipid compositions. In particular, the DH presented increased phosphatidic acid (PA) and decreased phosphatidylcholine (PC) compared to the VH, potentially implicating the phospholipase D (PLD) pathway in DH-VH axis regulation (Miranda et al., 2019). Moreover, PA levels were differently modulated by corticosterone, a known mediator of stress, suggesting differential recruitment of PA-modulating enzymes in pathological conditions (Miranda et al., 2019).

PLD encompasses a family of lipid-modifying enzymes primarily known for catabolizing PC to PA. Six PLD members (PLD1–PLD6) have been described in mammals, but only 2 isoenzymes with proposed canonical PLD activity have been reported, PLD1 and PLD2 (Frohman, 2015; Oliveira et al., 2010). PLD preferentially uses primary alcohols as a substrate, resulting in the formation of a specific phosphatidylalcohol, such as phosphatidylethanol (PEtOH) in the presence of ethanol, and this property has been used to measure PLD activity (Gustavsson, 1995; Oliveira et al., 2010; Scott et al., 2013). Despite PLD1

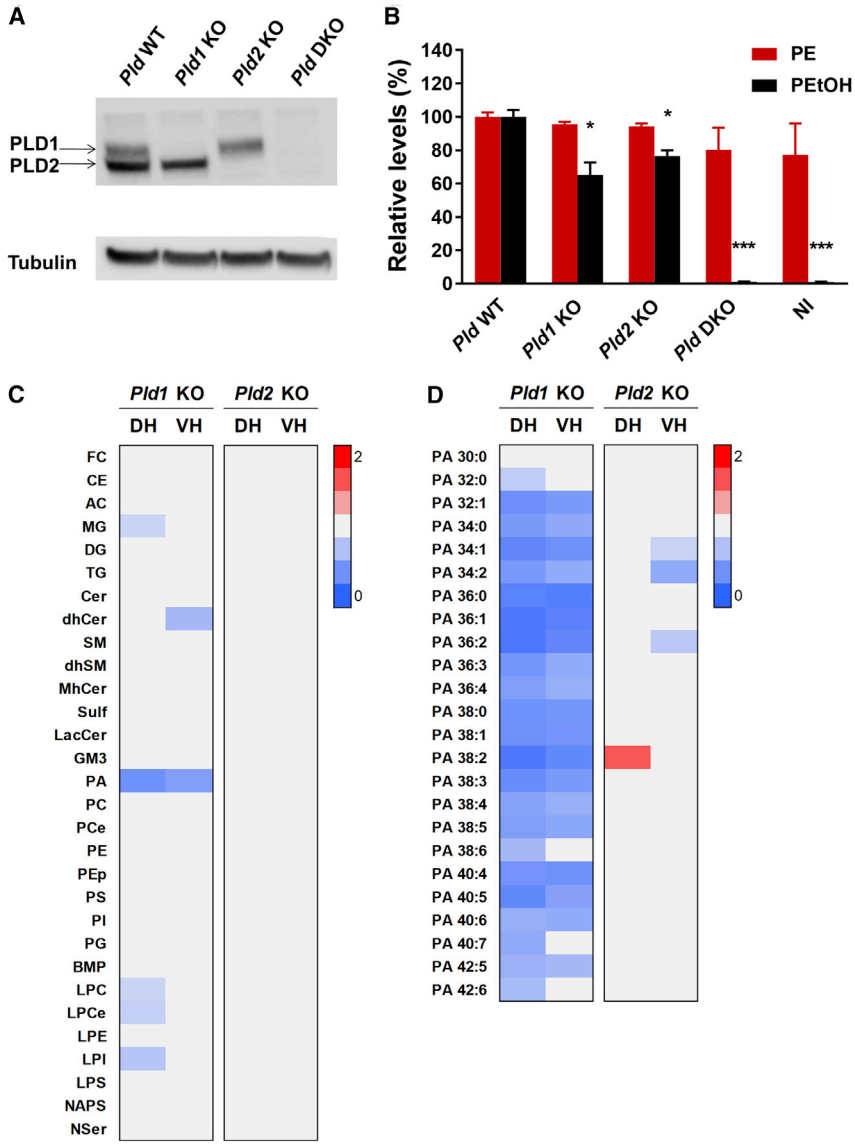

Figure 1. PLD1 Is a Major Contributor to Total Hippocampal PA Levels in Mice, and PLD1 Ablation Has a Major Impact on DH Lipidomics

(A) Forebrains from PLD-ablated mice were processed for western blot analysis. Specific PLD ablation leads to null levels of the corresponding protein.

(B) PLD enzymatic activity assessment. Mice were injected with ethanol, their forebrains were extracted, and the levels of PEtOH were measured by LC-MS analysis and used as an indicator of *in vivo* PLD activity. Individual lipid species were compared with corresponding WT mice (*Pld1* KO: unpaired t test $t(10) = 3.0216$, $p = 0.0129$; *Pld2* KO: unpaired t test $t(10) = 2.4982$, $p = 0.0315$; *Pld* DKO: unpaired t test $t(10) = 23.9625$, $p < 0.0001$; non-injected (NI): unpaired t test $t(9) = 11.9538$, $p < 0.0001$). PE was used as a control lipid. Values denote means ± SEMs ($n_{Pld\ WT} = 6$, $n_{Pld1\ KO} = 6$, $n_{Pld2\ KO} = 6$, $n_{Pld\ DKO} = 6$, $n_{Pld\ WT\ NI} = 5$).

(C) LC-MS analysis of DH and VH from *Pld1* KO and *Pld2* KO animals. In DH, PLD1 ablation decreases the total levels of PA (unpaired t test $t(10) = 7.3291$, $p < 0.0001$), MG (unpaired t test $t(10) = 2.3606$, $p = 0.0399$), LPC (unpaired t test $t(10) = 2.6934$, $p = 0.0226$), LPCe (unpaired t test $t(10) = 3.1084$, $p = 0.0111$), and LPI (unpaired t test $t(10) = 3.8857$, $p = 0.0030$). In VH, PLD1 ablation decreases the levels of PA (unpaired t test $t(10) = 5.4942$, $p = 0.0003$) and dhCer (unpaired t test $t(10) = 3.0964$, $p = 0.0113$).

(D) Impact of PLD1 or PLD2 ablation in specific PA species, analyzed by LC-MS.

Values are represented in gradient color: blue indicates <1 and red indicates above 1-fold change, respectively, normalized to WT mice ($n_{Pld1\ WT} = 5$, $n_{Pld1\ KO} = 7$, $n_{Pld2\ WT} = 8$, $n_{Pld2\ KO} = 8$) (C and D). DKO, *Pld* double-KO; PA, phosphatidic acid; PE, phosphatidylethanolamine; PEtOH, phosphatidylethanol. For other lipid nomenclature see Method Details. *$p < 0.05$, ***$p < 0.001$. See also Figures S1, S2, and S3 and Tables S1 and S2.

and PLD2 having similar enzymatic roles and structure, they differ in their intracellular localization and modulation (Frohman, 2015; Oliveira et al., 2010). Both PLD1 and PLD2 are expressed throughout brain development and postnatal life (Peng and Rhodes, 2000; Zhao et al., 1998), and conflicting results have been reported upon PLD1 or PLD2 ablation in mice behavior, showing either cognitive dysfunction (Burkhardt et al., 2014) or either minor or no major behavioral deficits (Oliveira et al., 2010; Vermeren et al., 2016). The PLD pathway has been implicated in Alzheimer's disease (AD) pathogenesis as being involved in amyloid beta (Aβ) signaling (Bravo et al., 2018; Oliveira et al., 2010) and amyloid precursor protein (APP) processing and trafficking (Cai et al., 2006a, 2006b).

Here, we show that PLD1 is a major source of PA in both rodent DH and VH compared to PLD2, which led us to further test the impact of PLD1 genetic ablation in the mouse hippocampus. We targeted dorsal-ventral hippocampal lipidomic gradient signatures and showed that PLD1 ablation differentially affects hippocampal organization and functioning in a region-specific manner, which has implications for disorders that affect learning and memory.

RESULTS

PLD1 and PLD2 Are the Only Contributors to Total PLD Activity in the Mouse Brain

To confirm the impact on the protein levels of each isoenzyme ablation and validate the genetic ablation of mice, western blot analysis was performed (Figure 1A) using an antibody that recognizes the COOH terminus of both PLD1 and PLD2 isoenzymes. Accordingly, in forebrain extracts, *Pld1* knockout (KO) animals express only PLD2, *Pld2* KO animals express only PLD1 enzyme, and *Pld* double-KO (DKO) animals have no PLD1 or PLD2 expression (Figure 1A). To study the impact of genetic ablation

on enzyme activity, an *in vivo* PLD activity assay was performed, relying on the ability to use primary alcohols—ethanol in this case—as nucleophiles over water in a transphosphatidylation reaction to generate PEtOH. Mice were injected with ethanol; after 1 h, lipid extraction was performed from forebrain tissue and PEtOH was measured by liquid chromatography-mass spectrometry (LC-MS) (Figure 1B). Both *Pld1* and *Pld2* KO mice showed a decrease in total PEtOH levels. Although the decrease in PLD activity was higher in *Pld1* KO animals, no significant differences were observed between *Pld1* and *Pld2* KO animals (Figure 1B). No significant changes were observed in control phospholipid phosphatidylethanolamine (PE) in *Pld1*, *Pld2*, or *Pld* DKO animals (Figure 1B). Also, *Pld* DKO showed almost no detectable PEtOH, which indicates that PEtOH is exclusively produced by PLD1 and PLD2 in the mouse forebrain. In agreement, non-injected animals presented virtually undetectable PEtOH levels (Figure 1B). At the lipid species level, of the 42 PEtOH species evaluated, 15 were significantly reduced in *Pld1* KO and 7 in *Pld2* KO (Figure S1). There were 4 PEtOH minor species, 32:2/16:1, 40:4/20:4, and 40:3/20:3, which were lower in the non-injected group, and 36:1/16:1, which was lower in the DKO. Although these species were significantly lower compared to *Pld* wild type (WT), they did not differ when we compared DKO and the non-injected group (Figure S1). The effect of ablating both PLD isoenzymes in *Pld* DKO on PEtOH levels was of greater magnitude (≈100% decrease) than adding the effects of PLD1 (≈35% decrease) and PLD2 (≈24% decrease) ablation (Figure 1B). Another intriguing observation was that *Pld2* KO forebrain presented increased levels of 4 PEtOH species, 38:4/20:4, 38:2/20:2, 38:2/20:1, and 38:1/20:1 (Figure S1), which was unexpected, considering that these are potential PLD enzymatic products, and indicates that PLD1 is overcompensating in the absence of PLD2. To explore the possibility of an expression compensatory process by either PLD1 or PLD2 upon each isoenzyme ablation, *Pld1*/PLD1 and *Pld2*/PLD2 mRNA and protein levels were measured (Figures S2 and S3). We observed that ablating either of the PLD isoenzymes does not lead to expression upregulation (Figures S2 and S3). These results show that both PLD1 and PLD2 contribute significantly to total PLD activity and that there are no other detectable canonical PLD activity sources in the mouse forebrain.

PLD1 Is a Major PA Source, and Its Ablation Has a Major Impact in the DH Lipidome

Next, we conducted a broad-scale, unbiased lipidomic profiling of DH and VH from both *Pld1* and *Pld2* WT and KO mice. We analyzed the relative abundance of a total of 30 lipid classes, covering the 3 main lipid categories of sterols, sphingolipids, and glycerophospholipids (Figure 1C; Table S1). We found that PLD2 ablation did not have a significant impact on the total levels of the lipid classes analyzed. However, PLD1 ablation led to a dramatic decrease in the total levels of PA in both DH and VH (Figure 1C; Table S1). PLD1 protein levels were higher in the DH when compared to the VH (Figure S3B). Of note, PLD1 ablation significantly decreased the levels of several lipid classes, with a higher impact on the DH compared to VH. The levels of monoacylglycerol (MG), lysophosphatidylcholine (LPC), ether lysophosphatidylcholine (LPCe), and lysophosphatidylinositol (LPI) were reduced in the DH, while levels of dihydroceramide (dhCer) were decreased in the VH (Figure 1C; Table S1). When analyzing the relative abundance of PA species, we found that PLD1 KO animals have decreased levels of nearly all PA species detected in both DH and VH (Figure 1D; Table S2), while PLD2 ablation leads to the decrease in only PA 34:1, 34:2, and 36:2 in the VH and an increase in PA 38:2 in DH (Figure 1D; Table S2). PA 34:1, the PA species with the most relative abundance (Table S2), decreased upon the ablation of either PLD1 or PLD2, and the second and third most abundant species, PA 36:1 and 38:4 (Table S2), only decreased in *Pld1* KO. These results indicate that PLD1 is a major contributor to total PA levels and that PLD1 ablation mainly affects the lipidome of the DH compared to the VH, which is in agreement with the higher PLD1 protein levels in the DH (Figure S3B).

PLD1 Ablation Impairs Object Recognition and Social Exploration in a Hippocampus-Dependent Social Discrimination Task

Knowing that PLD1 was a major contributor to PA total levels compared to PLD2, and since PLD1 ablation was associated with a greater impact in the dorsal-ventral hippocampal lipidome, we explored the impact of PLD1 ablation in hippocampal-associated behaviors. With the open field (OF) (Figure 2A) and elevated plus maze (EPM) (Figure 2B) tests, we observed that *Pld1* KO animals did not demonstrate significant locomotor or anxiety-like impairments. In fear memory evaluation, *Pld1* KO animals did not differ from WT in the average freezing percentage time in contextual or cued memory (Figure 2C, left panel). Also, the extinction of freezing percentage time upon cue exposure was unaltered both in the 5 subsequent days (Figure 2C, right panel) and 30 days later (Figure S4A). To further explore the impact on cognitive functions, the Morris water maze (MWM) was performed to assess spatial learning and reference memory, and *Pld1* KO animals showed preserved spatial learning (Figure 2D, left panel) and memory (Figure 2D, right panel). Moreover, *Pld1* KO animals showed no deficits in reaching a visually cued platform (Figure S4B). We then tested short-term memory, evaluated with the novel object recognition (NOR) test, and *Pld1* KO showed a reduction in the discrimination between familiar and novel objects, mainly at the expense of higher levels of exploration time of the familiar object (Figures 2E and S4C). To understand whether this impairment translated into other animal exploration deficits, the social discrimination, social preference, and preference for social novelty were tested (Figures 2F and S4D–S4F). Although PLD1 ablation did not significantly impair social preference (Figure S4E), the preference for social novelty (Figure S4F), or the ability to recognize a littermate (Figure 2F, left panel, and Figure S4D), *Pld1* KO animals were less social in a hippocampus-dependent task (Meira et al., 2018), since they spent less time exploring compared to WT (Figure 2F, right panel). We show here that PLD1 ablation causes deficits in an NOR task and impairs social behavior in a hippocampus-engaging task.

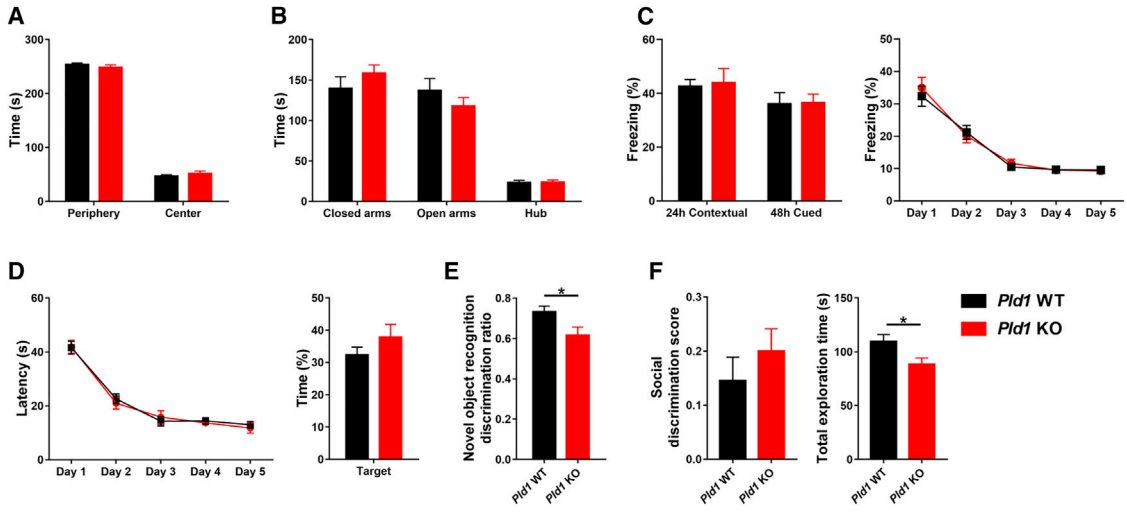

Figure 2. PLD1 Ablation Impairs Object Recognition and Social Exploration during a Social Discrimination Task

(A) The ablation of PLD1 does not have apparent consequences in locomotion, exploratory activity, and anxiety, as assessed by the OF test (n_{WT} = 25, n_{KO} = 23).

(B) *Pld1* KO mice exhibit no alterations in anxiety behavior when compared to WT, assessed by the EPM test (n_{WT} = 23, n_{KO} = 23).

(C) PLD1 ablation has no impact in contextual or cued fear conditioning (left panel) and no impact in the extinction protocol (right panel) (n_{WT} = 8, n_{KO} = 11).

(D) The ablation of PLD1 has no impact in spatial memory, evaluated with the MWM test. No differences were detected concerning spatial learning (left panel) and reference memory (right panel) in *Pld1* KO mice, compared to their WT littermates (n_{WT} = 23, n_{KO} = 20).

(*E*) *Pld1* KO mice deficits in object recognition-related short-term memory, evaluated with the NOR test (unpaired t test $t(29) = 2.315$, $p = 0.0279$). The discrimination ratio was calculated by dividing the time spent exploring the novel object by the time spent exploring both objects (n_{WT} = 16, n_{KO} = 15).

(F) *Pld1* KO mice are able to discriminate between a littermate and a strange mouse (left panel), but they spend less time interacting with conspecifics in a social discrimination task (left panel) (unpaired t test $t(37) = 2.432$, $p = 0.0200$). The social discrimination score was calculated as the difference between the time spent exploring the cups placed on the side chambers, divided by the total time exploring both (n_{WT} = 20, n_{KO} = 19).

Bars represent means ± SEMs. *$p < 0.05$. See also Figure S4.

PLD1 Ablation Disrupts DH-VH Dendritic Arborization Differentiation

Neuronal dendrites are crucial for information input, signal integration, and neuronal functioning. Since PLD1 has been implicated in dendritic arborization regulation (Ziegler and Tavosanis, 2019), we tested the impact of PLD1 ablation in dendritic branching in CA1 and CA3 pyramidal cells and dentate gyrus (DG) granule cells in both DH and VH. We observed multiple differences when comparing DH to VH in *Pld1* WT, such as decreased VH CA1 basal dendritic length (Figure 3A), decreased VH CA1 apical number of nodes (Figure 3A), increased CA3 VH basal dendritic length of VH (Figure 3B), decreased CA3 VH apical number of nodes (Figure 3B), and increased CA3 VH apical spine density (Figure 3B). These DH-VH differences in CA1–CA3 were not observed upon PLD1 ablation, which suggests that PLD1 is necessary for DH-VH structural differentiation. Also, when directly comparing genotypes, a decrease was observed in the apical dendritic length of CA3 DH of *Pld1* KO mice when compared to *Pld1* WT (Figure 3B). Finally, PLD1 ablation did not have a major impact on DH-VH structural differentiation in the DG (Figure 3C). These observations indicate that PLD1 is necessary for proper dendritic arborization organization and DH-VH structural differentiation, preferentially in both CA1 and CA3.

PLD1 Ablation Reduces LTD Induction in the DH

To further explore the importance of PLD1 in intra-hippocampal circuitry, *ex vivo* hippocampal extracellular electrophysiological recordings were performed upon Schaffer collateral stimulation and recording in CA1 to assess the impact of PLD1 ablation in synaptic plasticity paradigms, such as long-term potentiation (LTP) and long-term depression (LTD), in both the DH and VH (Figure 4). Assessment of LTP showed no major differences between *Pld1* WT and KO animals in either the DH or VH (Figure 4A). However, while there was no impact of PLD1 ablation in LTD in the VH, we observed a reduction in LTD induction in the DH of *Pld1* KO animals (Figure 4B). The input-output recordings and paired pulse facilitation revealed no differences between *Pld1* WT and KO mice in either the DH or VH (Figures 4C and S5). This shows that PLD1 is necessary for synaptic plasticity-associated LTD with a specific regional effect in the DH.

PLD1 Ablation Reduces GluN2A and SNAP-25 Levels in the DH

In light of specific DH-VH alterations at the lipidomic, behavioral, dendritic arborization, and electrophysiological levels, we further evaluated the impact of PLD1 ablation in the levels of proteins involved in synaptic function in both the DH and VH. We found that PLD1 ablation specifically leads to decreased SNAP-25 and GluN2A (also known as NR2A) protein levels in the DH (Figure 5). The levels of another presynaptic protein, synaptophysin, as well as other postsynaptic proteins, PSD95, Homer, GluA1 (also known as GluR1), GluA2 (also known as GluR2), GluN2B (also known as NR2B), and GluN2B-P (phosphorylated at Y1472), were not affected by PLD1 ablation at either the DH or

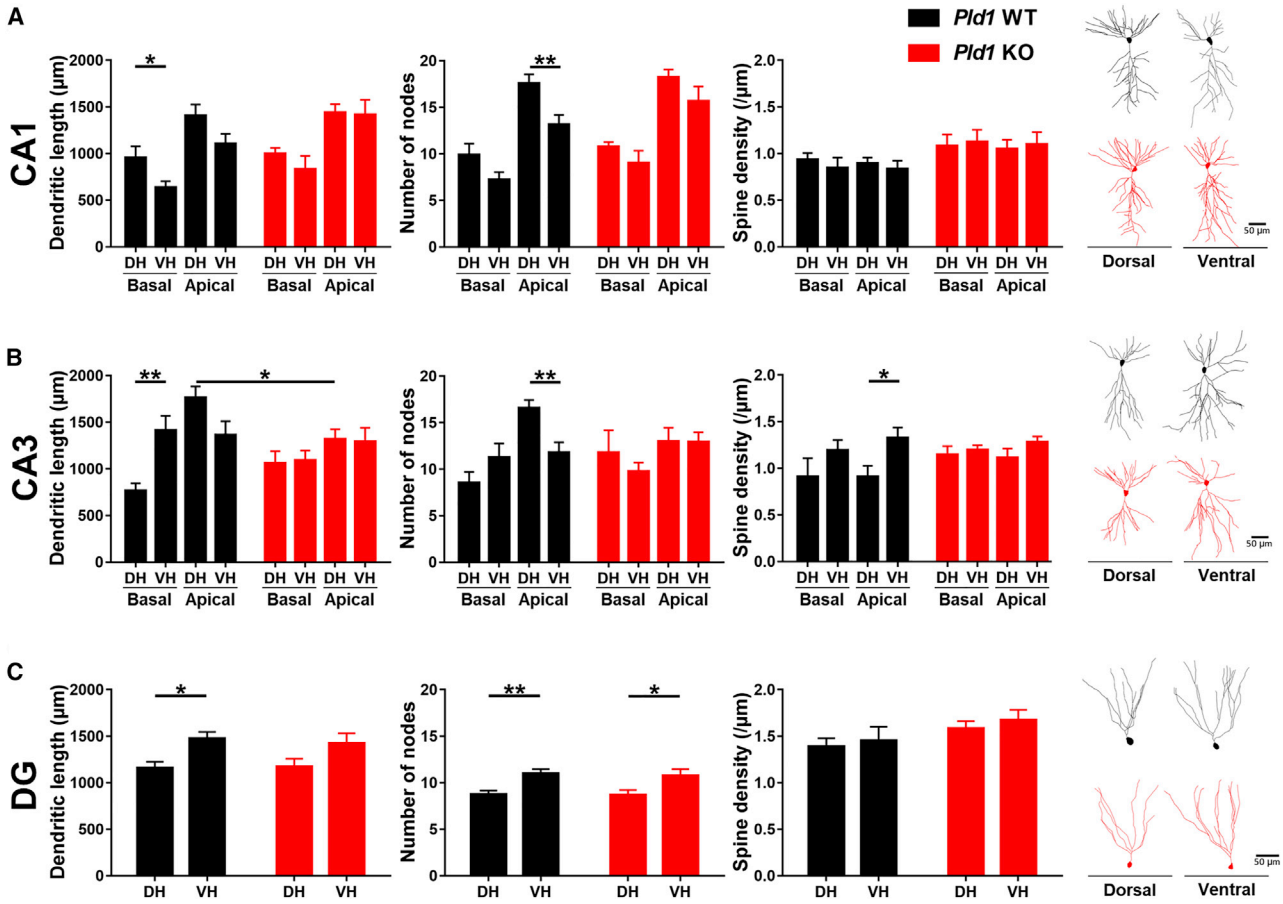

Figure 3. PLD1 Ablation Disrupts DH-VH Dendritic Arborization Differentiation

(A) In CA1 (n_{WT} = 8, n_{KO} = 6–7), there is a significant decrease in the basal dendritic length of VH when compared to DH in *Pld1* WT animals (unpaired t test $t(14)$ = 2.265, p = 0.0399). There is also a significant decrease in the apical number of nodes of VH when compared to DH in *Pld1* WT animals (unpaired t test $t(14)$ = 3.071, p = 0.0083).

(B) In CA3 (n_{WT} = 5–6, n_{KO} = 6), there is a significant increase in the basal dendritic length of VH when compared to DH in *Pld1* WT animals (unpaired t test $t(9)$ = 3.459, p = 0.0072). There is also a significant decrease in the apical number of nodes of VH when compared to DH in *Pld1* WT animals (unpaired t test $t(9)$ = 3.322, p = 0.0089). Moreover, there is a significant increase in the apical spine density of VH when compared to DH in *Pld1* WT animals (unpaired t test $t(9)$ = 2.503, p = 0.0337). Concerning the genotype, a decrease was observed in the apical dendritic length of CA3 DH of *Pld1* KO mice when compared to *Pld1* WT (unpaired t test $t(9)$ = 2.766, p = 0.0219).

(C) In DG (n_{WT} = 6–8, n_{KO} = 6–7), there is a significant increase in the dendritic length of VH when compared to DH in *Pld1* WT animals (unpaired t test $t(13)$ = 3.38, p = 0.0049). There is also a significant increase in the number of nodes of VH when compared to DH in *Pld1* WT animals (unpaired t test $t(13)$ = 3.613, p = 0.0032), which is reproduced when PLD1 is ablated (unpaired t test $t(12)$ = 2.342, p = 0.0372).

Bars represent means ± SEMs. *p < 0.05, **p < 0.01.

VH (Figure 5). Given the observed changes in SNAP-25, we also tested whether other SNARE complex proteins were altered and observed no changes in syntaxin-1A and synaptobrevin-2 protein levels upon PLD1 ablation (Figure 5). GluA1, GluN2A, and GluN2B-P levels were found to be higher in DH compared to VH in *Pld1* WT animals, and while this DH-VH difference persisted for GluA1 upon PLD1 ablation, it was not observed for GluN2A and GluN2B-P (Figure 5). Moreover, the levels of syntaxin-1A were higher in the VH when compared to the DH (Figure 5). Overall, it shows that PLD1 reduction leads to a specific reduction in the DH of SNAP-25 and GluN2A protein levels, which could partially explain the synaptic plasticity changes observed in LTD and disrupted DH-VH segregation.

DISCUSSION

Based on anatomical, gene expression, and functional studies, the hippocampus presents an organized gradient along its longitudinal axis, which highlights the differential contribution of its DH and VH poles to physiological and pathological processes linked to mood regulation, learning, and memory (Strange et al., 2014). In light of recent lipidomic observations suggesting that PA and the PLD pathway could be differentially regulated along the DH-VH axis (Miranda et al., 2019; Pavel et al., 2019), we tested the impact of PLD genetic modulation on the DH-VH axis organization and function. We found that PLD1 is the major contributor for total PA production in the mouse forebrain, when

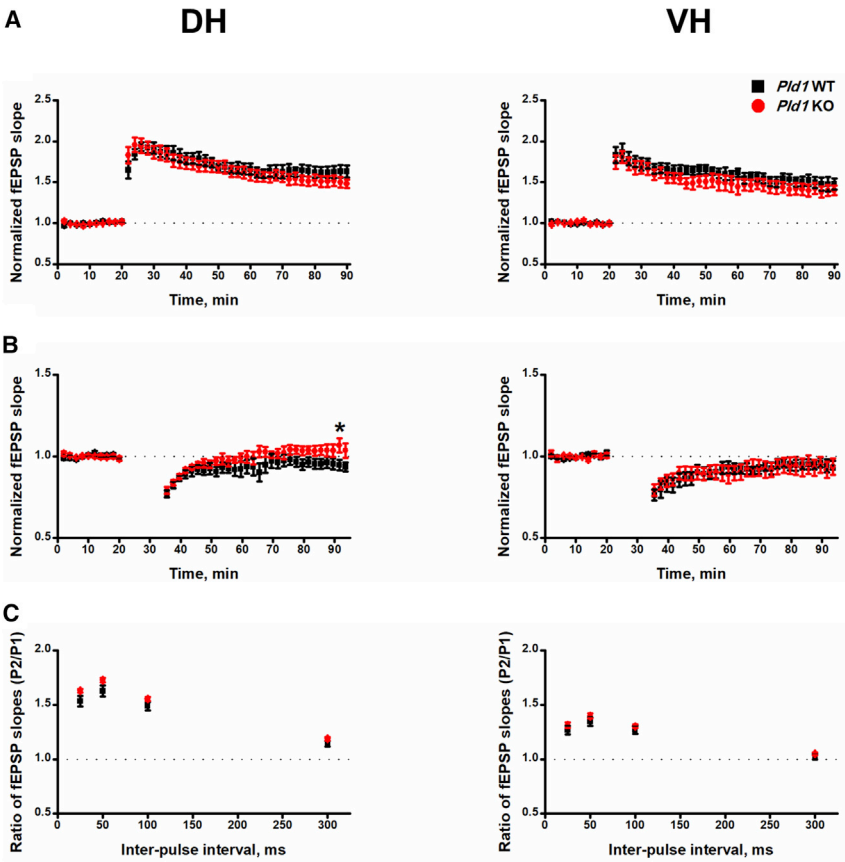

Figure 4. PLD1 Ablation Reduces LTD in the DH

(A) LTP was measured in acute slices of DH (left panel) (n_{WT} = 9, n_{KO} = 8) and VH (right panel) (n_{WT} = 8, n_{KO} = 8).

(B) LTD was measured in acute slices of DH (left panel) (n_{WT} = 9, n_{KO} = 9) and VH (right panel) (n_{WT} = 7, n_{KO} = 8). There was an increase in excitability in the late phase of LTD of DH in *Pld1* KO animals (unpaired t test $t(16) = 2.143$, $p = 0.0478$).

(C) Paired pulse (PP) ratios in acute slices of DH (left panel) (n_{WT} = 18, n_{KO} = 14) and VH (right panel) (n_{WT} = 14, n_{KO} = 14). Within WT animals, 2-way ANOVA showed the PP curves of DH and VH to be different (2-way ANOVA: interaction $F(3,90) = 11.7$, $p < 0.0001$; WT DH/VH $F(1,30) = 16.8$, $p = 0.0003$). The bars represent means ± SEMs. fEPSP, field excitatory postsynaptic potential. *$p < 0.05$.

See also Figure S5.

compared to PLD2, affecting predominantly the DH lipidome. We further showed that PLD1 ablation leads to a CA1/CA3 dendritic arborization reorganization, to behavioral deficits in novelty recognition and social interaction, to deficits in DH LTD, and to specific synaptic protein alterations predominantly in the DH. Thus, we show that PLD1 is necessary for the proper organization and function of the longitudinal hippocampal axis, with a preferential impact in the DH. In this study, we used adult mice, and since *Pld1* expression is high during brain development (Colley et al., 1997), we cannot exclude the possibility that our observations in adult mice could be affected by an early PLD deficit.

To study the impact of modulating the PLD pathway, we measured PLD activity in the forebrains of *Pld1* KO, *Pld2* KO, and *Pld* DKO animals by quantifying PEtOH levels after ethanol injection (Figures 1B and S1). Both *Pld1* and *Pld2* KO show decreased levels of acutely produced forebrain PEtOH (Figures 1B and S1). However, although both PLD1 and PLD2 synthesize PA, PLD1 ablation had a higher-magnitude impact than PLD2 in basal hippocampal PA levels (Figures 1C and 1D), which is in accordance with other recent observations (Liang et al., 2019). The added reducing effect on total PLD activity upon the ablation of either PLD1 (≈35%) and PLD2 (≈24%) does not add up to the near-absence of detectable levels of total PLD activity in *Pld* DKO animals (Figure 1B), which is highly likely due to compensatory mechanisms on both *Pld1* and *Pld2* KO animals. Our data suggest that these compensatory mechanisms do not occur by isoenzyme translation upregulation (Figures S2 and S3); other possibilities are that the activity upregulation could be due to altered localization, post-translational modifications, or differences in co-factor modulation (Selvy et al., 2011). Moreover, the PA and PEtOH species profile analysis suggests that PLD1 and PLD2 modulate different PA pools. While PLD1 affects both shorter and longer fatty acyl carbon length PA species, PLD2 modulates predominantly shorter fatty acyl carbon length PA species (Figures 1D and S1). Overall, these results are somewhat in accordance with previous observations that show no changes in total PA levels upon PLD2 ablation (Oliveira et al., 2010; Vermeren et al., 2016) and a differential effect on various PA species, demonstrating also in some instances an increase in specific PA species (Oliveira et al., 2010; Vermeren et al., 2016), which is likely induced by a compensatory PLD1 response. At the species level, the most consistent change we observed upon PLD2 ablation was the decrease in PA/PEtOH 34:2 (Figures 1 and S1). However, other previously reported decreases in PA 32:1 and 38:4 and increase in PA 32:0 levels (Oliveira et al., 2010) were not observed here, although differences in the analyzed brain regions and mouse age should be accounted for. Increased PLD activity has been proposed to be detrimental and has been implicated in neurodegeneration either by an Aβ-induced overactive state in the context of AD (Oliveira et al., 2010) or by overexpressing PLD in the fly rhabdomere (Raghu et al., 2009), with specific increased levels in PA 34:2 in both cases. In a particular experimental setting with cultured neutrophils, PLD1 or PLD2 ablation only unraveled its PLD-dependent phenotypes upon activating conditions (Norton et al., 2011). Since we observe here compensatory crosstalk between each isoenzyme, it will be relevant in future studies targeting PLD1 or PLD2, by genetic or pharmacological means, to consider the observed phenotypes not only as a loss of

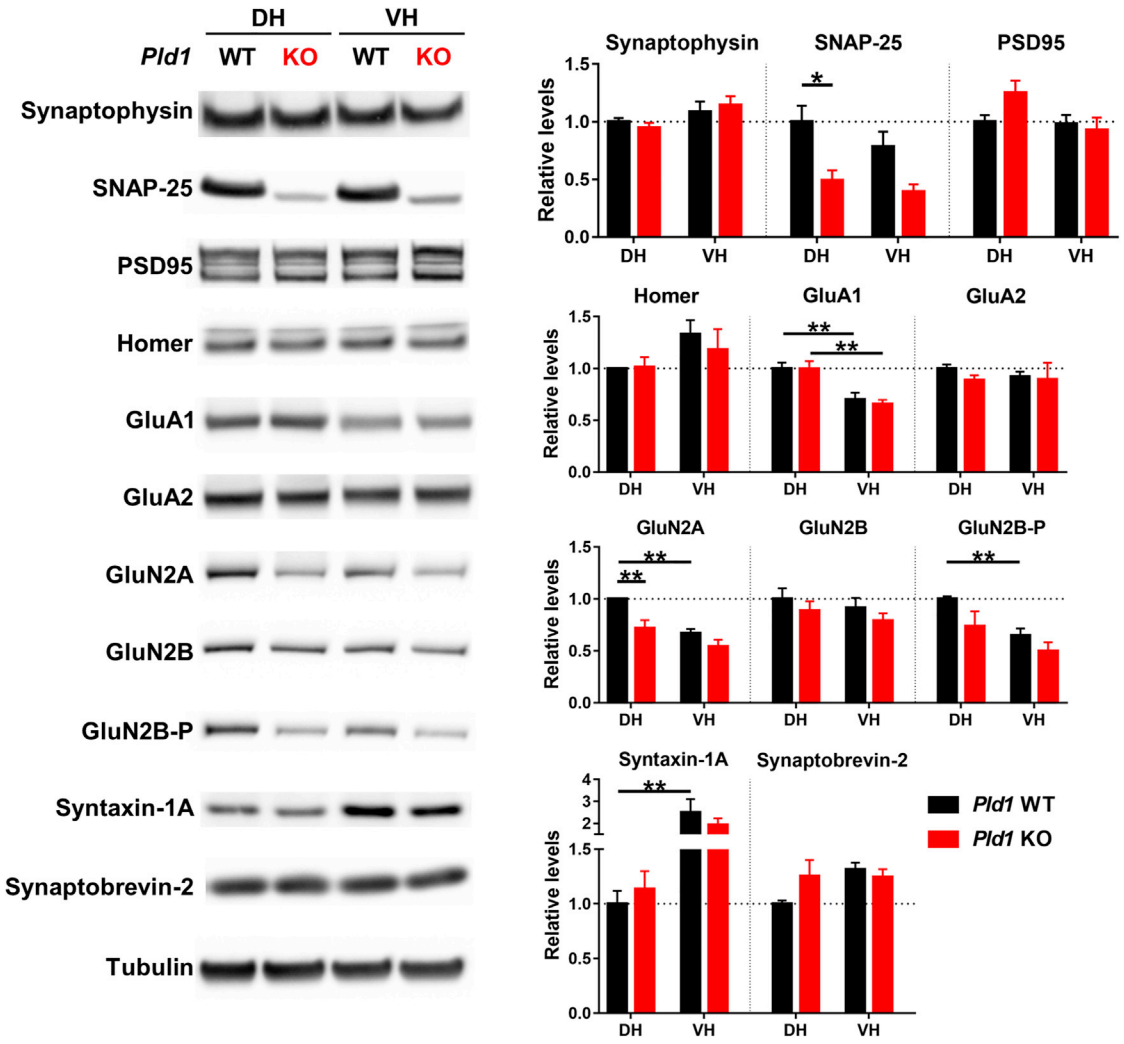

Figure 5. PLD1 Ablation Reduces GluA2 and SNAP-25 Levels in DH

Protein levels of DH and VH were evaluated by western blot analysis and quantified by densitometric analysis (n = 5–9). PLD1 ablation decreased the levels of GluA2 (2-way ANOVA: interaction $F(1,24) = 2.007$, $p = 0.1695$; WT/KO $F(1,24) = 13.73$, $p = 0.0011$; DH WT/KO $p = 0.0070$, Tukey's multiple comparisons test) and SNAP-25 in the DH (2-way ANOVA: interaction $F(1,32) = 0.2838$, $p = 0.5979$; WT/KO $F(1,32) = 16.91$, $p = 0.0003$; DH WT/KO: $p = 0.0126$; Tukey's multiple comparisons test). There was a decrease in GluA1 levels when comparing VH with DH in *Pld1* WT animals. This difference persisted with PLD1 ablation (2-way ANOVA: interaction $F(1,32) = 0.1318$, $p = 0.7190$; DH/VH $F(1,32) = 29.55$, $p < 0.0001$; WT DH/VH $p = 0.0058$; KO DH/VH $p = 0.0014$; Tukey's multiple comparisons test). In *Pld1* WT animals, the levels of GluA2 (2-way ANOVA: interaction $F(1,24) = 2.007$, $p = 0.1695$; DH/VH $F(1,24) = 20.95$, $p = 0.0001$; WT DH/VH $p = 0.0015$; Tukey's multiple comparisons test) and the levels of Glu2B-P (2-way ANOVA: interaction $F(1,28) = 0.3767$, $p = 0.5443$; DH/VH $F(1,28) = 10.79$, $p = 0.0027$; WT DH/VH $p = 0.0472$; Tukey's multiple comparisons test) were decreased in the VH when compared to DH. The levels of syntaxin-1A were increased in the VH when compared to DH in WT animals (2-way ANOVA: interaction $F(1,20) = 1.013$, $p = 0.3261$; DH/VH $F(1,20) = 10.76$, $p = 0.0037$; WT DH/VH $p = 0.0309$; Tukey's multiple comparisons test). Individual protein levels were compared with WT DH. GluN2B-P is phosphorylated at Y1472. Representative blots are shown. The bars represent means ± SEMs. For some points, the error bars are not drawn since they would be shorter than the height of the symbol. *$p < 0.05$, **$p < 0.01$.

function effect but also as a potential gain of function through a compensatory activation of its isoenzyme counterpart. This takes on further importance in light of differential signaling factors that regulate the functioning of either PLD1 or PLD2, or alternatively, that PLD co-factors, such as $PI(4,5)P_2$, could be differentially affected by altered PA synthesis by either PLD1 or PLD2 (Selvy et al., 2011).

Another observation that can be inferred from our PLD activity studies is that PLD1 and PLD2 are likely the only canonical PLD isoenzymes. While the PLD superfamily also includes PLD3–PLD6, which have in common the presence of HKD domains (Barber et al., 2018; Nelson and Frohman, 2015), our data indicate that these other members do not contribute to the production of PEtOH. This is relevant because the PLD pathway has been implicated in AD pathogenesis (Oliveira and Di Paolo, 2010), with reported effects of PLD1 on APP processing and trafficking (Cai et al., 2006a, 2006b) and PLD2 on Aβ downstream pathological signaling (Oliveira et al., 2010). Since human genetic studies implicated PLD3 as a potential risk factor for AD (Cruchaga et al., 2014), the recent understanding of its role in

lysosomal function (Fazzari et al., 2017; Gonzalez et al., 2018) raises the question of whether PLD3 functioning is directly connected to PLD1 or PLD2 AD pathophysiology. Both PLD3 and PLD4 were found to be exonucleases regulating the inflammatory cytokine response (Gavin et al., 2018), which could be linked to the multiple genetic AD risk factors connected to immune system biology (Karch and Goate, 2015).

Concerning the impact of reducing PLD levels on other lipid classes, the ablation of PLD1, but not PLD2, had a significant effect, with greater repercussions in the DH when compared to the VH, mainly affecting lysoglycerophospholipids such as LPC, LPCe, and LPI (Figure 1C). This suggests potential crosstalk between different phospholipases, namely PLA2, which is a main lysoglycerophospholipid source (Burke and Dennis, 2009). Co-expression phospholipase studies showed that PLD2, but not PLD1, augmented PLA2 activity (Ueno et al., 2000), which could in part justify the observed lipidomic alterations in the DH in a hypothetical PLD2 recruitment in a PLD1 ablation condition.

Knowing that PLD1 ablation had a more significant effect on the hippocampal lipidome than did PLD2 ablation, we focused more specifically on studying *Pld1* KO mice. From the multitude of behavioral tests that we covered in *Pld1* KO animals, we observed a deficit only in short-term NOR (Figure 2E) and in the social interaction time in a hippocampal-dependent social discrimination task (Figure 2F). This is partially in accordance with another report in which PLD1 ablation shows a trend toward a deficit in the level of discrimination in long-term NOR and a social recognition deficit (Burkhardt et al., 2014). While the same authors also observed deficits in social and object recognition in *Pld2* KO animals (Burkhardt et al., 2014), others showed that PLD2 ablation had no major behavioral deficits (Oliveira et al., 2010; Vermeren et al., 2016), besides an olfaction deficit in aged mice (Vermeren et al., 2016). Overall, these studies indicate that even though PLD isoenzyme ablation is somewhat manageable by the organism, future approaches should take into account not only the mouse strain used, age, and sex but also the contribution of each isoenzyme specifically in experimental conditions that lead to on-demand PLD activation unraveling specific phenotypes, such as the case of the protective effect observed upon PLD2 ablation in an AD mouse model (Oliveira et al., 2010).

Considering the previously described gradient of PA in the long hippocampal axis with higher PA levels in the DH (Miranda et al., 2019), and since PLD1 is a major PA source (Figure 1), we hypothesized that PLD1 could play an important role in hippocampal dendritic organization. Here, we observed a marked structural DH-VH differentiation of CA1/CA3 dendritic arborization in *Pld1* WT animals, and these differences were essentially absent upon PLD1 ablation (Figures 3A and 3B). Opposing effects on dendritic arborization have been reported upon PLD1 ablation. Some authors showed that *Pld1* KO cultured neurons had decreased dendritic branching (Ammar et al., 2013), while others observed the opposite effect upon reducing PLD1 levels (Zhu et al., 2012). More recently, using mixed neuronal and astrocyte cultures, it was shown that PLD1 reduces PA in astrocytes, reducing protein kinase A activation in neurons and consequently dendritic branching (Zhu et al., 2016). Therefore, the specific role of PLD1 in dendritic arborization and its regulatory factors are still being debated. One plausible possibility is that PA, acting as a fusogenic lipid due to its inverted cone-shaped structure, could differentially contribute to membrane addition in different neurite outgrowth conditions (Tanguy et al., 2019).

At the functional level, we observed that PLD1 ablation reduced LTD induction in the DH CA1 after low-frequency stimulation (LFS) at the Schaffer collaterals, while it had no effects in the VH, unraveling a specific effect along the longitudinal hippocampal axis (Figure 4). Recently, it was shown that PLD1 is necessary for LTD induction in the mouse prefrontal cortex, which phenocopies our observations in the DH (Moran et al., 2019). Along with the observed deficits in NOR in *Pld1* KO animals (Figure 2E), it was previously shown that hippocampal LTD induction was associated with the recognition of novel objects (Kemp and Manahan-Vaughan, 2004). Also, lipid signaling has previously been observed to be involved in LTD mechanisms; aligned with that, not only were arachidonic acid metabolites shown to induce LTD (Feinmark et al., 2003) but also PLA2 inhibition was shown to block LTD in neonatal hippocampal slices (Fitzpatrick and Baudry, 1994). Since we observe here that PLD1 ablation reduces various lysoglycerophospholipid levels in the DH (Figure 1C), it further supports that PLA2 could be in a hypoactive state, partially explaining why LTD induction was reduced upon PLD1 ablation. Another possibility is based on the findings that PA binds and activates phosphatidylinositol 4-phosphate 5-kinase (PIP5K) (Jenkins et al., 1994; Stace et al., 2008), which was shown to be necessary for LFS LTD induction (Unoki et al., 2012). Moreover, since hippocalcin was shown to be necessary for LTD induction (Palmer et al., 2005) and to activate PLD (Hyun et al., 2000; Oh et al., 2006), these observations are coherent with a role for the PLD pathway in LTD-associated plasticity mechanisms, even if the contribution for each PLD isoenzyme should still be addressed. Finally, PLD1 has been shown in *in vitro* neuron culture experiments to be involved in other synaptic plasticity-associated pathways. For instance, it was proposed that PLD1-derived PA activates the mammalian target of rapamycin (mTOR), affecting its synaptic plasticity regulation in a chemical LTP setting with an impact in brain-derived neurotrophic factor (BDNF) dendritic expression levels (Henry et al., 2018). Also, PLD1 was shown to act as a BDNF downstream effector necessary for the phosphorylation of both mTOR and cAMP response element-binding protein (CREB) (Ammar et al., 2013). Overall, these specific pathway regulations could be relevant for other brain regions or could be specific in certain experimental settings, taking into account the complex circuitry and different cell types in an *in vivo-ex vivo* experimental approach.

To gain further insight into the molecular pathways affected by PLD1 ablation, we assessed different synaptic protein levels both in DH and VH (Figure 5). The dendritic DH-VH differences in WT animals occur in parallel with higher protein levels of GluN2A, GluN2B-P (phosphorylated at Y1472), and GluA1 in DH (Figure 5). Accordingly, tyrosine phosphorylation of GluN2B has been reported to regulate the number of dendritic spines and morphological changes (Wang et al., 2018), an autism

spectrum disorder-associated mutation in GluN2B leads to dendritic abnormal development (Sceniak et al., 2019), dendritic branch pruning along maturation is accompanied by an elevation in GluN2A levels (Bustos et al., 2014), GluN2A genetic ablation was shown to reduce dendritic length in dentate granule cells (Kannangara et al., 2014), and GluA1 expression was shown to promote dendritic branching (Zhou et al., 2008). The most intriguing observation was the marked reduction in the target N-ethylmaleimide-sensitive fusion protein attachment protein receptor (t-SNARE) protein SNAP-25 in the DH of *Pld1* KO animals (Figure 5). The SNAP-25 yeast ortholog Spo20p was reported to bind to PA (Liu et al., 2007). Taking advantage of this property, Spo20p is regularly used as a PA probe and was found to co-localize with mammalian SNAP-25 in an experimental context of acutely activated exocytosis (Zeniou-Meyer et al., 2007). Moreover, SNAP-25 was reported to bind to anionic lipids, such as PA, and even though, to our knowledge, PA binding was not specifically tested, SNAP-25 was found to bind to $PI(4,5)P_2$, which PA could still indirectly modulate by PIP5K activation (Jenkins et al., 1994; Stace et al., 2008). Although the reduction of SNAP-25 levels led to deficits in sociability behavior and susceptibility to pharmacologically induced seizures, it partially phenocopied *Pld1* KO animals, which also show deficits in NOR and social interaction in a hippocampus-specific task (Figure 2) and no deficits in spatial learning and memory tasks (Corradini et al., 2014). Moreover, infusion with a C-terminal SNAP-25 fragment, proposed to block its normal functions, reduces CA3-CA1 LTD induction (Zhang et al., 2011), and reduction in SNAP-25 levels also leads to deficits in LTD induction in corticostriatal preparations (Baca et al., 2013). Since the functions of SNAP-25 have been described at both the presynaptic (Bronk et al., 2007) and postsynaptic (Fossati et al., 2015) compartments, both possibilities should be considered when studying the impact of PLD1-derived PA on SNAP-25 functioning. Also, since SNAP-25 is a member of the soluble SNARE complex (Ramakrishnan et al., 2012), we tested the impact on other SNARE complex proteins, such as syntaxin-1A and synaptobrevin-2, and no changes were observed upon PLD1 ablation in either the DH or VH (Figure 5).

In summary, our work shows that lipid signaling modulation differently affects the hippocampus along its longitudinal axis. We show that PLD1 ablation predominantly affects the DH, with implications for disorders that affect learning and memory, such as AD and mood disorders. Moreover, we observe that PLD1 ablation reduces SNAP-25 levels, and since SNAP-25 has been implicated in attention-deficit/hyperactivity disorder (Feng et al., 2005), autism spectrum disorders (Guerini et al., 2011), and schizophrenia (Thompson et al., 2003), it further highlights the potential role of lipid signaling dysregulation in these neuropsychiatric disorders.

STAR★METHODS

Detailed methods are provided in the online version of this paper and include the following:

- KEY RESOURCES TABLE
- LEAD CONTACT AND MATERIALS AVAILABITY
- EXPERIMENTAL MODEL AND SUBJECT DETAILS
- METHOD DETAILS
  - Western Blot
  - *In vivo* PLD activity
  - Lipid Analysis
  - Behavioral testing
  - Dendritic Arborization
  - Electrophysiology
  - Gene expression analysis by qRT-PCR
- QUANTIFICATION AND STATISTICAL ANALYSIS
- DATA AND CODE AVAILABILITY

SUPPLEMENTAL INFORMATION

Supplemental Information can be found online at https://doi.org/10.1016/j.celrep.2020.02.102.

ACKNOWLEDGMENTS

This work was supported by grants from the Portuguese North Regional Operational Program (ON.2, O Novo Norte) under the National Strategic Reference Framework (QREN), through the European Regional Development Fund, European Union (FEDER); the Fundação para a Ciência e Tecnologia, Portugal (PD/BD/105915/2014 to A.M.M.), Norte2020 (UMINHO/BD/52/2017 to L.S.-M.); the Ruth L. Kirschstein National Research Service Award F31 Individual Fellowship (1F31NS073387-01 to K.P.d.J.); and the BIAL Foundation, Portugal (253/14 to T.G.O.). We thank Sung Ho Ryu (Pohang University of Science and Technology, South Korea) for providing the PLD antibody. We appreciate the contributions of João Carlos Gonçalves (University of Minho, Portugal), Inês Xavier Fernandes (University of Minho, Portugal), Sónia Guerra-Gomes (University of Minho, Portugal), and Jorge Da Silva (University of Minho, Portugal) for help with the behavioral analysis. We thank Clarissa Waites (Columbia University, USA), Luís Santos (Mount Sinai Hospital, USA), and Catarina Ferreira (Mount Sinai Hospital, USA) for help in acquiring reagents. We thank Carlos Bandeira Duarte (University of Coimbra, Portugal), Patrícia Monteiro (University of Minho, Portugal), and João Carlos Sousa (University of Minho, Portugal) for scientific discussions and critical input relevant to this project.

AUTHOR CONTRIBUTIONS

T.G.O. conceived the idea. T.G.O. acquired the core funding for the work. L.S.-M., I.C., and T.G.O. designed and planned the experiments. L.S.-M. and I.C. performed the majority of the experiments. V.P. coordinated and supervised the electrophysiological experiments. R.R.S. and F.V.B. contributed to the behavioral analysis and preliminary experiments. T.M. contributed to the planning and the behavioral analysis. R.M.-R. and F.M. contributed to the RT-PCR experiments. L.S.-M., A.M.M., Y.X., K.P.d.J., M.W., R.B.C., G.D.P., and T.G.O. contributed to the lipidomic experiments. L.S.-M. and T.G.O. wrote the paper, and all of the authors reviewed and edited the manuscript.

DECLARATION OF INTERESTS

G.D.P. is a full-time employee of Denali Therapeutics. G.D.P. and T.G.O. are listed as inventors on the patent number WO2010138869A1, "Modulation of Phospholipase D for the Treatment of Neurodegenerative Disorders." R.B.C., G.D.P., and T.G.O. are listed as inventors on the patent number US20120302604A1, "Modulation of Phospholipase D for the Treatment of the Acute and Chronic Effects of Ethanol."

Received: September 17, 2019
Revised: January 29, 2020
Accepted: February 27, 2020
Published: March 24, 2020

REFERENCES

Ammar, M.R., Humeau, Y., Hanauer, A., Nieswandt, B., Bader, M.F., and Vitale, N. (2013). The Coffin-Lowry syndrome-associated protein RSK2 regulates neurite outgrowth through phosphorylation of phospholipase D1 (PLD1) and synthesis of phosphatidic acid. J. Neurosci. *33*, 19470–19479.

Baca, M., Allan, A.M., Partridge, L.D., and Wilson, M.C. (2013). Gene-environment interactions affect long-term depression (LTD) through changes in dopamine receptor affinity in Snap25 deficient mice. Brain Res. *1532*, 85–98.

Bannerman, D.M., Sprengel, R., Sanderson, D.J., McHugh, S.B., Rawlins, J.N., Monyer, H., and Seeburg, P.H. (2014). Hippocampal synaptic plasticity, spatial memory and anxiety. Nat. Rev. Neurosci. *15*, 181–192.

Barber, C.N., Huganir, R.L., and Raben, D.M. (2018). Phosphatidic acid-producing enzymes regulating the synaptic vesicle cycle: role for PLD? Adv. Biol. Regul. *67*, 141–147.

Bienkowski, M.S., Bowman, I., Song, M.Y., Gou, L., Ard, T., Cotter, K., Zhu, M., Benavidez, N.L., Yamashita, S., Abu-Jaber, J., et al. (2018). Integration of gene expression and brain-wide connectivity reveals the multiscale organization of mouse hippocampal networks. Nat. Neurosci. *21*, 1628–1643.

Bligh, E.G., and Dyer, W.J. (1959). A rapid method of total lipid extraction and purification. Can. J. Biochem. Physiol. *37*, 911–917.

Bravo, F.V., Da Silva, J., Chan, R.B., Di Paolo, G., Teixeira-Castro, A., and Oliveira, T.G. (2018). Phospholipase D functional ablation has a protective effect in an Alzheimer's disease Caenorhabditis elegans model. Sci. Rep. *8*, 3540.

Bronk, P., Deák, F., Wilson, M.C., Liu, X., Südhof, T.C., and Kavalali, E.T. (2007). Differential effects of SNAP-25 deletion on Ca2+ -dependent and Ca2+ -independent neurotransmission. J. Neurophysiol. *98*, 794–806.

Burke, J.E., and Dennis, E.A. (2009). Phospholipase A2 biochemistry. Cardiovasc. Drugs Ther. *23*, 49–59.

Burkhardt, U., Stegner, D., Hattingen, E., Beyer, S., Nieswandt, B., and Klein, J. (2014). Impaired brain development and reduced cognitive function in phospholipase D-deficient mice. Neurosci. Lett. *572*, 48–52.

Bustos, F.J., Varela-Nallar, L., Campos, M., Henriquez, B., Phillips, M., Opazo, C., Aguayo, L.G., Montecino, M., Constantine-Paton, M., Inestrosa, N.C., and van Zundert, B. (2014). PSD95 suppresses dendritic arbor development in mature hippocampal neurons by occluding the clustering of NR2B-NMDA receptors. PLoS One *9*, e94037.

Cai, D., Netzer, W.J., Zhong, M., Lin, Y., Du, G., Frohman, M., Foster, D.A., Sisodia, S.S., Xu, H., Gorelick, F.S., and Greengard, P. (2006a). Presenilin-1 uses phospholipase D1 as a negative regulator of beta-amyloid formation. Proc. Natl. Acad. Sci. USA *103*, 1941–1946.

Cai, D., Zhong, M., Wang, R., Netzer, W.J., Shields, D., Zheng, H., Sisodia, S.S., Foster, D.A., Gorelick, F.S., Xu, H., and Greengard, P. (2006b). Phospholipase D1 corrects impaired betaAPP trafficking and neurite outgrowth in familial Alzheimer's disease-linked presenilin-1 mutant neurons. Proc. Natl. Acad. Sci. USA *103*, 1936–1940.

Chan, R.B., Oliveira, T.G., Cortes, E.P., Honig, L.S., Duff, K.E., Small, S.A., Wenk, M.R., Shui, G., and Di Paolo, G. (2012). Comparative lipidomic analysis of mouse and human brain with Alzheimer disease. J. Biol. Chem. *287*, 2678–2688.

Colley, W.C., Altshuller, Y.M., Sue-Ling, C.K., Copeland, N.G., Gilbert, D.J., Jenkins, N.A., Branch, K.D., Tsirka, S.E., Bollag, R.J., Bollag, W.B., and Frohman, M.A. (1997). Cloning and expression analysis of murine phospholipase D1. Biochem. J. *326*, 745–753.

Corradini, I., Donzelli, A., Antonucci, F., Welzl, H., Loos, M., Martucci, R., De Astis, S., Pattini, L., Inverardi, F., Wolfer, D., et al. (2014). Epileptiform activity and cognitive deficits in SNAP-25(+/−) mice are normalized by antiepileptic drugs. Cereb. Cortex *24*, 364–376.

Cruchaga, C., Karch, C.M., Jin, S.C., Benitez, B.A., Cai, Y., Guerreiro, R., Harari, O., Norton, J., Budde, J., Bertelsen, S., et al.; Alzheimer's Research UK (ARUK) Consortium (2014). Rare coding variants in the phospholipase D3 gene confer risk for Alzheimer's disease. Nature *505*, 550–554.

Dall'Armi, C., Hurtado-Lorenzo, A., Tian, H., Morel, E., Nezu, A., Chan, R.B., Yu, W.H., Robinson, K.S., Yeku, O., Small, S.A., et al. (2010). The phospholipase D1 pathway modulates macroautophagy. Nat. Commun. *1*, 142.

Fanselow, M.S., and Dong, H.W. (2010). Are the dorsal and ventral hippocampus functionally distinct structures? Neuron *65*, 7–19.

Fazzari, P., Horre, K., Arranz, A.M., Frigerio, C.S., Saito, T., Saido, T.C., and De Strooper, B. (2017). PLD3 gene and processing of APP. Nature *541*, E1–E2.

Feinmark, S.J., Begum, R., Tsvetkov, E., Goussakov, I., Funk, C.D., Siegelbaum, S.A., and Bolshakov, V.Y. (2003). 12-lipoxygenase metabolites of arachidonic acid mediate metabotropic glutamate receptor-dependent long-term depression at hippocampal CA3-CA1 synapses. J. Neurosci. *23*, 11427–11435.

Feng, Y., Crosbie, J., Wigg, K., Pathare, T., Ickowicz, A., Schachar, R., Tannock, R., Roberts, W., Malone, M., Swanson, J., et al. (2005). The SNAP25 gene as a susceptibility gene contributing to attention-deficit hyperactivity disorder. Mol. Psychiatry *10*, 998–1005, 973.

Fitzpatrick, J.S., and Baudry, M. (1994). Blockade of long-term depression in neonatal hippocampal slices by a phospholipase A2 inhibitor. Brain Res. Dev. Brain Res. *78*, 81–86.

Fossati, G., Morini, R., Corradini, I., Antonucci, F., Trepte, P., Edry, E., Sharma, V., Papale, A., Pozzi, D., Defilippi, P., et al. (2015). Reduced SNAP-25 increases PSD-95 mobility and impairs spine morphogenesis. Cell Death Differ. *22*, 1425–1436.

Frohman, M.A. (2015). The phospholipase D superfamily as therapeutic targets. Trends Pharmacol. Sci. *36*, 137–144.

Gavin, A.L., Huang, D., Huber, C., Mårtensson, A., Tardif, V., Skog, P.D., Blane, T.R., Thinnes, T.C., Osborn, K., Chong, H.S., et al. (2018). PLD3 and PLD4 are single-stranded acid exonucleases that regulate endosomal nucleic-acid sensing. Nat. Immunol. *19*, 942–953.

Gibb, R., and Kolb, B. (1998). A method for vibratome sectioning of Golgi-Cox stained whole rat brain. J. Neurosci. Methods *79*, 1–4.

Gonzalez, A.C., Schweizer, M., Jagdmann, S., Bernreuther, C., Reinheckel, T., Saftig, P., and Damme, M. (2018). Unconventional Trafficking of Mammalian Phospholipase D3 to Lysosomes. Cell Rep. *22*, 1040–1053.

Guerini, F.R., Bolognesi, E., Chiappedi, M., Manca, S., Ghezzo, A., Agliardi, C., Sotgiu, S., Usai, S., Matteoli, M., and Clerici, M. (2011). SNAP-25 single nucleotide polymorphisms are associated with hyperactivity in autism spectrum disorders. Pharmacol. Res. *64*, 283–288.

Gustavsson, L. (1995). ESBRA 1994 Award Lecture. Phosphatidylethanol formation: specific effects of ethanol mediated via phospholipase D. Alcohol Alcohol. *30*, 391–406.

Henry, F.E., Wang, X., Serrano, D., Perez, A.S., Carruthers, C.J.L., Stuenkel, E.L., and Sutton, M.A. (2018). A Unique Homeostatic Signaling Pathway Links Synaptic Inactivity to Postsynaptic mTORC1. J. Neurosci. *38*, 2207–2225.

Hyun, J.K., Yon, C., Kim, Y.S., Noh, D.Y., Lee, K.H., and Han, J.S. (2000). Role of hippocalcin in Ca2+ -induced activation of phospholipase D. Mol. Cells *10*, 669–677.

Jenkins, G.H., Fisette, P.L., and Anderson, R.A. (1994). Type I phosphatidylinositol 4-phosphate 5-kinase isoforms are specifically stimulated by phosphatidic acid. J. Biol. Chem. *269*, 11547–11554.

Kannangara, T.S., Bostrom, C.A., Ratzlaff, A., Thompson, L., Cater, R.M., Gil-Mohapel, J., and Christie, B.R. (2014). Deletion of the NMDA receptor GluN2A subunit significantly decreases dendritic growth in maturing dentate granule neurons. PLoS One *9*, e103155.

Karch, C.M., and Goate, A.M. (2015). Alzheimer's disease risk genes and mechanisms of disease pathogenesis. Biol. Psychiatry *77*, 43–51.

Kemp, A., and Manahan-Vaughan, D. (2004). Hippocampal long-term depression and long-term potentiation encode different aspects of novelty acquisition. Proc. Natl. Acad. Sci. USA *101*, 8192–8197.

Kheirbek, M.A., Drew, L.J., Burghardt, N.S., Costantini, D.O., Tannenholz, L., Ahmari, S.E., Zeng, H., Fenton, A.A., and Hen, R. (2013). Differential control of learning and anxiety along the dorsoventral axis of the dentate gyrus. Neuron *77*, 955–968.

Leger, M., Quiedeville, A., Bouet, V., Haelewyn, B., Boulouard, M., Schumann-Bard, P., and Freret, T. (2013). Object recognition test in mice. Nat. Protoc. *8*, 2531–2537.

Liang, D., Wu, K., Tei, R., Bumpus, T.W., Ye, J., and Baskin, J.M. (2019). A real-time, click chemistry imaging approach reveals stimulus-specific subcellular locations of phospholipase D activity. Proc. Natl. Acad. Sci. USA *116*, 15453–15462.

Liu, S., Wilson, K.A., Rice-Stitt, T., Neiman, A.M., and McNew, J.A. (2007). In vitro fusion catalyzed by the sporulation-specific t-SNARE light-chain Spo20p is stimulated by phosphatidic acid. Traffic *8*, 1630–1643.

Maggio, N., and Segal, M. (2007). Striking variations in corticosteroid modulation of long-term potentiation along the septotemporal axis of the hippocampus. J. Neurosci. *27*, 5757–5765.

McHugh, S.B., Fillenz, M., Lowry, J.P., Rawlins, J.N., and Bannerman, D.M. (2011). Brain tissue oxygen amperometry in behaving rats demonstrates functional dissociation of dorsal and ventral hippocampus during spatial processing and anxiety. Eur. J. Neurosci. *33*, 322–337.

Meira, T., Leroy, F., Buss, E.W., Oliva, A., Park, J., and Siegelbaum, S.A. (2018). A hippocampal circuit linking dorsal CA2 to ventral CA1 critical for social memory dynamics. Nat. Commun. *9*, 4163.

Miranda, A.M., Bravo, F.V., Chan, R.B., Sousa, N., Di Paolo, G., and Oliveira, T.G. (2019). Differential lipid composition and regulation along the hippocampal longitudinal axis. Transl. Psychiatry *9*, 144.

Moran, S.P., Xiang, Z., Doyle, C.A., Maksymetz, J., Lv, X., Faltin, S., Fisher, N.M., Niswender, C.M., Rook, J.M., Lindsley, C.W., and Conn, P.J. (2019). Biased M_1 receptor-positive allosteric modulators reveal role of phospholipase D in M_1-dependent rodent cortical plasticity. Sci. Signal. *12*, eaax2057.

Moy, S.S., Nadler, J.J., Young, N.B., Perez, A., Holloway, L.P., Barbaro, R.P., Barbaro, J.R., Wilson, L.M., Threadgill, D.W., Lauder, J.M., et al. (2007). Mouse behavioral tasks relevant to autism: phenotypes of 10 inbred strains. Behav. Brain Res. *176*, 4–20.

Nelson, R.K., and Frohman, M.A. (2015). Physiological and pathophysiological roles for phospholipase D. J. Lipid Res. *56*, 2229–2237.

Norton, L.J., Zhang, Q., Saqib, K.M., Schrewe, H., Macura, K., Anderson, K.E., Lindsley, C.W., Brown, H.A., Rudge, S.A., and Wakelam, M.J. (2011). PLD1 rather than PLD2 regulates phorbol-ester-, adhesion-dependent and Fcgamma-receptor-stimulated ROS production in neutrophils. J. Cell Sci. *124*, 1973–1983.

Oh, D.Y., Yon, C., Oh, K.J., Lee, K.S., and Han, J.S. (2006). Hippocalcin increases phospholipase D2 expression through extracellular signal-regulated kinase activation and lysophosphatidic acid potentiates the hippocalcin-induced phospholipase D2 expression. J. Cell. Biochem. *97*, 1052–1065.

Oliveira, T.G., and Di Paolo, G. (2010). Phospholipase D in brain function and Alzheimer's disease. Biochim. Biophys. Acta *1801*, 799–805.

Oliveira, T.G., Chan, R.B., Tian, H., Laredo, M., Shui, G., Staniszewski, A., Zhang, H., Wang, L., Kim, T.W., Duff, K.E., et al. (2010). Phospholipase d2 ablation ameliorates Alzheimer's disease-linked synaptic dysfunction and cognitive deficits. J. Neurosci. *30*, 16419–16428.

Oliveira, T.G., Chan, R.B., Bravo, F.V., Miranda, A., Silva, R.R., Zhou, B., Marques, F., Pinto, V., Cerqueira, J.J., Di Paolo, G., and Sousa, N. (2016). The impact of chronic stress on the rat brain lipidome. Mol. Psychiatry *21*, 80–88.

Palmer, C.L., Lim, W., Hastie, P.G., Toward, M., Korolchuk, V.I., Burbidge, S.A., Banting, G., Collingridge, G.L., Isaac, J.T., and Henley, J.M. (2005). Hippocalcin functions as a calcium sensor in hippocampal LTD. Neuron *47*, 487–494.

Pavel, M.A., Petersen, E.N., Wang, H., Lerner, R.A., and Hansen, S.B. (2019). Studies on the mechanism of membrane mediated general anesthesia. bioRxiv. https://doi.org/10.1101/313973.

Peng, J.F., and Rhodes, P.G. (2000). Developmental expression of phospholipase D2 mRNA in rat brain. Int. J. Dev. Neurosci. *18*, 585–589.

Pinto, V., Costa, J.C., Morgado, P., Mota, C., Miranda, A., Bravo, F.V., Oliveira, T.G., Cerqueira, J.J., and Sousa, N. (2015). Differential impact of chronic stress along the hippocampal dorsal-ventral axis. Brain Struct. Funct. *220*, 1205–1212.

Raghu, P., Coessens, E., Manifava, M., Georgiev, P., Pettitt, T., Wood, E., Garcia-Murillas, I., Okkenhaug, H., Trivedi, D., Zhang, Q., et al. (2009). Rhabdomere biogenesis in Drosophila photoreceptors is acutely sensitive to phosphatidic acid levels. J. Cell Biol. *185*, 129–145.

Ramakrishnan, N.A., Drescher, M.J., and Drescher, D.G. (2012). The SNARE complex in neuronal and sensory cells. Mol. Cell. Neurosci. *50*, 58–69.

Sceniak, M.P., Fedder, K.N., Wang, Q., Droubi, S., Babcock, K., Patwardhan, S., Wright-Zornes, J., Pham, L., and Sabo, S.L. (2019). An autism-associated mutation in GluN2B prevents NMDA receptor trafficking and interferes with dendrite growth. J. Cell Sci. *132*, jcs232892.

Scott, S.A., Xiang, Y., Mathews, T.P., Cho, H.P., Myers, D.S., Armstrong, M.D., Tallman, K.A., O'Reilly, M.C., Lindsley, C.W., and Brown, H.A. (2013). Regulation of phospholipase D activity and phosphatidic acid production after purinergic (P2Y6) receptor stimulation. J. Biol. Chem. *288*, 20477–20487.

Selvy, P.E., Lavieri, R.R., Lindsley, C.W., and Brown, H.A. (2011). Phospholipase D: enzymology, functionality, and chemical modulation. Chem. Rev. *111*, 6064–6119.

Shah, S., Lubeck, E., Zhou, W., and Cai, L. (2017). seqFISH Accurately Detects Transcripts in Single Cells and Reveals Robust Spatial Organization in the Hippocampus. Neuron *94*, 752–758.e1.

Stace, C., Manifava, M., Delon, C., Coadwell, J., Cockcroft, S., and Ktistakis, N.T. (2008). PA binding of phosphatidylinositol 4-phosphate 5-kinase. Adv. Enzyme Regul. *48*, 55–72.

Strange, B.A., Witter, M.P., Lein, E.S., and Moser, E.I. (2014). Functional organization of the hippocampal longitudinal axis. Nat. Rev. Neurosci. *15*, 655–669.

Tanguy, E., Wang, Q., Moine, H., and Vitale, N. (2019). Phosphatidic Acid: From Pleiotropic Functions to Neuronal Pathology. Front. Cell. Neurosci. *13*, 2.

Thompson, P.M., Egbufoama, S., and Vawter, M.P. (2003). SNAP-25 reduction in the hippocampus of patients with schizophrenia. Prog. Neuropsychopharmacol. Biol. Psychiatry *27*, 411–417.

Thompson, C.L., Pathak, S.D., Jeromin, A., Ng, L.L., MacPherson, C.R., Mortrud, M.T., Cusick, A., Riley, Z.L., Sunkin, S.M., Bernard, A., et al. (2008). Genomic anatomy of the hippocampus. Neuron *60*, 1010–1021.

Ueno, N., Murakami, M., and Kudo, I. (2000). Functional crosstalk between phospholipase D(2) and signaling phospholipase A(2)/cyclooxygenase-2-mediated prostaglandin biosynthetic pathways. FEBS Lett. *475*, 242–246.

Unoki, T., Matsuda, S., Kakegawa, W., Van, N.T., Kohda, K., Suzuki, A., Funakoshi, Y., Hasegawa, H., Yuzaki, M., and Kanaho, Y. (2012). NMDA receptor-mediated PIP5K activation to produce $PI(4,5)P_2$ is essential for AMPA receptor endocytosis during LTD. Neuron *73*, 135–148.

Vermeren, M.M., Zhang, Q., Smethurst, E., Segonds-Pichon, A., Schrewe, H., and Wakelam, M.J. (2016). The Phospholipase D2 Knock Out Mouse Has Ectopic Purkinje Cells and Suffers from Early Adult-Onset Anosmia. PLoS One *11*, e0162814.

Vorhees, C.V., and Williams, M.T. (2006). Morris water maze: procedures for assessing spatial and related forms of learning and memory. Nat. Protoc. *1*, 848–858.

Walf, A.A., and Frye, C.A. (2007). The use of the elevated plus maze as an assay of anxiety-related behavior in rodents. Nat. Protoc. *2*, 322–328.

Wang, X.Y., Zhou, H.R., Wang, S., Liu, C.Y., Qin, G.C., Fu, Q.Q., Zhou, J.Y., and Chen, L.X. (2018). NR2B-Tyr phosphorylation regulates synaptic plasticity in central sensitization in a chronic migraine rat model. J. Headache Pain *19*, 102.

Zeniou-Meyer, M., Zabari, N., Ashery, U., Chasserot-Golaz, S., Haeberlé, A.M., Demais, V., Bailly, Y., Gottfried, I., Nakanishi, H., Neiman, A.M., et al. (2007). Phospholipase D1 production of phosphatidic acid at the plasma membrane promotes exocytosis of large dense-core granules at a late stage. J. Biol. Chem. *282*, 21746–21757.

Zhang, X.L., Upreti, C., and Stanton, P.K. (2011). $G\beta\gamma$ and the C terminus of SNAP-25 are necessary for long-term depression of transmitter release. PLoS One *6*, e20500.

Zhao, D., Berse, B., Holler, T., Cermak, J.M., and Blusztajn, J.K. (1998). Developmental changes in phospholipase D activity and mRNA levels in rat brain. Brain Res. Dev. Brain Res. *109*, 121–127.

Zhou, W., Zhang, L., Guoxiang, X., Mojsilovic-Petrovic, J., Takamaya, K., Sattler, R., Huganir, R., and Kalb, R. (2008). GluR1 controls dendrite growth through its binding partner, SAP97. J. Neurosci. *28*, 10220–10233.

Zhu, Y.B., Kang, K., Zhang, Y., Qi, C., Li, G., Yin, D.M., and Wang, Y. (2012). PLD1 Negatively Regulates Dendritic Branching. J. Neurosci. *32*, 7960–7969.

Zhu, Y.B., Gao, W., Zhang, Y., Jia, F., Zhang, H.L., Liu, Y.Z., Sun, X.F., Yin, Y., and Yin, D.M. (2016). Astrocyte-derived phosphatidic acid promotes dendritic branching. Sci. Rep. *6*, 21096.

Ziegler, A.B., and Tavosanis, G. (2019). Glycerophospholipids - Emerging players in neuronal dendrite branching and outgrowth. Dev. Biol. *451*, 25–34.

STAR★METHODS

KEY RESOURCES TABLE

REAGENT or RESOURCE	SOURCE	IDENTIFIER
Antibodies		
Alpha-Tubulin (Figure 1)	Sigma-Aldrich	Cat# T5168, RRID:AB_477579
Alpha-Tubulin (Figure 5)	Sigma-Aldrich	Cat#T6074, RRID:AB_477582
GAPDH	Cell Signaling Technology	Cat# 2118, RRID:AB_561053
Phospholipase D	Made in house; Provided by Sung Ho Ryu (Pohang University of Science and Technology)	N/A
Phospholipase D1	Cell Signaling Technology	Cat# 3832, RRID:AB_2172256
Phospholipase D2 (N-term)	Abgent	Cat# AP14669a, RRID:AB_11135353
Synaptophysin 1	Synaptic Systems	Cat# 101 002, RRID:AB_887905
SNAP-25	Abcam	Cat# ab5666, RRID:AB_305033
PSD95	Abcam	Cat# ab2723, RRID:AB_303248
Homer	Abcam	Cat# ab184955, RRID:AB_2744679
GluA1 / GluR1	Millipore	Cat# AB1504, RRID:AB_2113602
GluA2 / GluR2	Abcam	Cat# ab133477, RRID:AB_2620181
GluN2A / NR2A	Millipore	Cat# AB1555P, RRID:AB_90770
GluN2B / NR2B	Abcam	Cat# ab65783, RRID:AB_1658870
pY1472-GluN2B / -NR2B	Abcam	Cat# ab3856, RRID:AB_304114
Syntaxin-1A	Synaptic Systems	Cat# 110 302, RRID:AB_887846
Synaptobrevin-2	Synaptic Systems	Cat# 104 202, RRID:AB_887810
Goat Anti-rabbit IgG	Bio-Rad	Cat# 170-6515, RRID:AB_11125142
Goat Anti-mouse IgG	Bio-Rad	Cat# 170-6516, RRID:AB_11125547
Chemicals, Peptides, and Recombinant Proteins		
cOmplete, Mini, EDTA-free Protease Inhibitor Cocktail	Roche	Cat#11836170001
Phosphatase Inhibitor Cocktail 2	Sigma-Aldrich	Cat#P5726
Phosphatase Inhibitor Cocktail 3	Sigma-Aldrich	Cat#P0044
NuPAGE Sample Reducing Agent	Invitrogen	Cat#NP0009
NuPAGE LDS Sample Buffer	Invitrogen	Cat#NP0007
NuPAGE 4-12% Bis-Tris Protein Gels	Invitrogen	Cat#NP0322
NuPAGE MES SDS Running Buffer	Invitrogen	Cat#NP0002
Amersham Protran Premium 0.45 NC nitrocellulose western blotting membranes	GE Healthcare Life Sciences	Cat# GE10600008
Clarity Western ECL Substrate	Bio-Rad	Cat#1705060
SuperSignal West Femto Maximum Sensitivity Substrate	ThermoFisher Scientific	Cat#34095
TRIzol reagent	Life Technologies, Thermo Fisher Scientific	Cat# 15596018
Critical Commercial Assays		
Pierce BCA protein assay	ThermoFisher Scientific	Cat#23225
iScript cDNA Synthesis Kit	Bio-Rad	Cat#1708891
HOT FIREPol EvaGreen qPCR Mix Plus (ROX) Kit	Solys Biodine	Cat# 08-24-00020
Experimental Models: Organisms/Strains		
Mouse: Pld1$^{tm1.1Gdp}$/J	Provided by Gilbert Di Paolo (Columbia University)	Available at Jackson laboratory Cat#028665; RRID:IMSR_JAX:028665
Mouse: B6.Cg-$^{Pld2tm1.1Gdp}$/J	Provided by Gilbert Di Paolo (Columbia University)	Available at Jackson laboratory Cat#028668; RRID:IMSR_JAX:028668

(*Continued on next page*)

Continued

REAGENT or RESOURCE	SOURCE	IDENTIFIER
Oligonucleotides		
Primer for qRT-PCR: Phospholipase D1 (*PLD1*) - Forward (5′→3′): CATCGACAGCACCTCCAAC	Stab Vida	N/A
Primer for qRT-PCR: Phospholipase D1 (*PLD1*) - Reverse (5′→3′): GAGTTCTCCCACTCCGGTCT	Stab Vida	N/A
Primer for qRT-PCR: Phospholipase D2 (*PLD2*) - Forward (5′→3′): TGGGTGACCCCTCTGAACCTGT	Stab Vida	N/A
Primer for qRT-PCR: Phospholipase D2 (*PLD2*) - Reverse (5′→3′): GTCCAGCTGCACCCAGTCCTT	Stab Vida	N/A
Primer for qRT-PCR: Heat Shock Protein 90 alpha family class B member 1 (*Hsp90ab1*) - Forward (5′→3′): GCTGGCTGAGGACAAGGAGA	Stab Vida	N/A
Primer for qRT-PCR: Heat Shock Protein 90 alpha family class B member 1 (*Hsp90ab1*) - Reverse (5′→3′): CGTCGGTTAGTGGAATCTTCATG	Stab Vida	N/A
Software and Algorithms		
ImageJ	NIH	RRID:SCR_003070
Prism	Graphpad	RRID:SCR_002798
MED-PC IV	Med Associates Inc.	N/A
Neurolucida software	MBF Bioscience	RRID:SCR_001775
NeuroExplorer software	MBF Bioscience	N/A
WinLTP software	WinLTP Ltd. and The University of Bristol	RRID:SCR_008590
Primer Blast	NCBI	RRID:SCR_003095
7500 Real-Time PCR Software	Applied Biosystems	RRID:SCR_014596

LEAD CONTACT AND MATERIALS AVAILABITY

Further information and requests for resources and reagents should be directed to and will be fulfilled by the Lead Contact, Tiago Gil Oliveira (tiago@med.uminho.pt). This study did not generate new unique reagents.

EXPERIMENTAL MODEL AND SUBJECT DETAILS

Pld1$^{-/-}$ mice were originally generated through the removal of exons 13 (that codes for the first HKD motif for PLD1) and 14, using a Cre-lox/FLP-FRT recombination system, as previously described (Dall'Armi et al., 2010). Using the same system, *Pld2*$^{-/-}$ mice were produced as a result of the elimination of exons 13-15, including exon 14 (that encodes for the first HKD motif of PLD2 as well), as shown before (Oliveira et al., 2010). The animals had C57BL/6 background with exception of the animals used in the experiments of Figures 1A and 1B that had mixed background (C57BL/6-129svj). Littermate mice were used in all experiments, except for experiments of Figures 1A and 1B. For the generation of *Pld1*$^{-/-}$ / *Pld2*$^{-/-}$ (DKO) mice, *Pld1*$^{-/-}$ animals were crossed with *Pld2*$^{-/-}$ animals. All experimental procedures were performed in compliance with the Portuguese authority for animal experimentation, *Direção Geral de Alimentação e Veterinária* (DGAV), the Directive 2010/63/EU guidelines and approved by the local committee. All mice had *ad libitum* access to water and food and maintained on a 12h light/dark cycle. All the procedures were performed during daytime, except for the social discrimination, sociability and preference for social novelty behavioral tests. Before all behavioral tests, animals were placed in the testing room one hour prior to testing, so they could acclimatize. The arenas and apparatus were cleaned with a 10% ethanol solution between testing subjects. 3-4 months male and female mice were used in all tests, except for western blot analysis (3-6 months), fear conditioning (males 3-7 months old) and social discrimination, sociability and preference for social novelty tests (males 3-6 months).

METHOD DETAILS

Western Blot

Animals were sacrificed by cervical dislocation and forebrain or the hippocampus were dissected. Hippocampi were divided in approximately three equal dorsal, intermediate and ventral parts. Samples were diluted in radioimmunoprecipitation assay buffer

(RIPA) containing 150 nM NaCl, 1.0% Triton X-100, 0.5% sodium deoxycholate, 0.1% SDS, 50 mM TrisBase pH = 8 and supplemented with protease (Roche) and phosphatase inhibitor cocktails (Sigma-Aldrich). After homogenization, samples were mixed in a rotator at 4°C for 2 hours at 40rpm and then centrifuged at 4°C for 20 minutes at 14000rpm. Supernatants were quantified (BCA, Pierce) and samples diluted to equal concentration in RIPA. Samples were prepared with NuPAGE LDS sample buffer and NuPAGE reducing reagent and loaded in NuPAGE 4%–12% Bis–Tris gels. MES SDS running buffer (NuPAGE) was used for separation. Wet transfer used 50% running buffer, 20% methanol and 30% deionized water and was made on 0.45μm nitrocellulose membranes (Amersham) for 2 hours at 100V. Membrane blockage was performed with 5% dried milk (Nestle) for 1 hour at room temperature. Incubation with primary antibodies, diluted in 2.5% dried milk or bovine serum albumin (BSA), was performed overnight at 4°C and incubation with HRP-conjugated secondary antibodies, diluted in 2.5% dried milk or BSA, was performed for 1 hour at room temperature. Chemiluminescence signal was detected with ChemiDoc XRS+ (Bio-Rad) and membrane development was achieved with Clarity Western ECL Substrate (Bio-Rad) or SuperSignal West Femto Maximum Sensitivity Substrate (ThermoScientific). Quantification was performed with ImageJ software. Primary antibodies used were: α-Tubulin (T5168, Sigma-Aldrich 1:10000) – Figure 1A; α-Tubulin (T6074, Sigma-Aldrich, 1:10000); GAPDH (Cell Signaling Technology, 1:3000); Antibody to the COOH terminus of PLD (kind gift of Dr. Sung Ho Ryu, Pohang University of Science and Technology; 1:200); PLD1 (Cell Signaling Technology, 1:500); PLD2 (Abgent, 1:500), Synaptophysin (Synaptic Systems, 1:5000); SNAP-25 (Abcam, 1:5000); PSD95 (Abcam, 1:5000); Homer (Abcam, 1:3000); GluA1/GluR1 (Millipore, 1:1000); GluA2/GluR2 (Abcam, 1:1000); GluN2A/NR2A (Millipore, 1:1000); GluN2B/NR2B (Abcam, 1:1000), pY1472-GluN2B/NR2B (Abcam, 1:1000), Syntaxin-1A (Synaptic Systems, 1:1000) and Synaptobrevin-2 (Synaptic Systems, 1:4000). HRP-conjugated secondary antibodies used were: Goat Anti-rabbit IgG (BioRad) and Goat Anti-mouse IgG (BioRad).

In vivo PLD activity

In the presence of primary alcohols, PLD utilizes preferentially short-chain alcohols as substrates resulting in the formation of the corresponding phosphatidylalcohol. This property was used to measure PLD activity. Mice were injected intraperitoneally with 3g/kg ethanol and sacrificed 1 hour postinjection, as previously described (Oliveira et al., 2010). Briefly, lipid extracts were prepared from mice whole forebrain using a modified Bligh and Dyer method (described below). The levels of PEtOH produced via a PLD-specific transphosphatidylation reaction were measured by LC-MS analysis (described below) and used as an indicator of *in vivo* PLD activity. Individual lipid species from *Pld1* KO, *Pld2* KO and *Pld* DKO mice were compared with wild-type (WT) mice. Phosphatydilethanolamine (PE) measurements were used as reference levels.

Lipid Analysis

Lipids were extracted using a modified Bligh and Dyer method (Bligh and Dyer, 1959) and lipid analysis performed as previously described (Chan et al., 2012; Miranda et al., 2019). Briefly, samples were homogenenized in a solution of methanol:chloroform (2:1) and lipids extracted with a solution of chloroform:KCl (3:2, 1 M). Samples were centrifuged at 4°C for 2 minutes at 9000rpm and the bottom phase (organic) was dried under vacuum nitrogen and stored at −80°C. Lipid extracts of purified microsome were spiked with a cocktail of internal standards and analyzed using a 6490 Triple Quadrupole LC/MS system (Agilent Technologies). Glycerophospholipids and sphingolipids were separated with normal-phase HPLC as described before (Chan et al., 2012), with a few modifications. An Agilent Zorbax Rx-Sil column (inner diameter 2.1 × 100 mm) was used under the following conditions: mobile phase A (chloroform:methanol:1 M ammonium hydroxide, 89.9:10:0.1, v/v) and mobile phase B (chloroform:methanol:water:ammonium hydroxide, 55:39.9:5:0.1, v/v); 95% A for 2 min, linear gradient to 30% A over 18 min and held for 3 min, and linear gradient to 95% A over 2 min and held for 6 min. Quantification of lipid species was accomplished using multiple reaction monitoring (MRM) transitions and instrument settings that were determined in earlier studies (Chan et al., 2012) in conjunction with referencing of known amounts of internal standards: PA 14:0/14:0, PC 14:0/14:0, PE 14:0/14:0, PI 12:0/13:0, PS 14:0/14:0, SM d18:1/12:0, (Avanti Polar Lipids). Nomenclature abbreviations are FC, free cholesterol; CE, cholesteryl ester; AC, acyl carnitine; MG, monoacylglycerol; DG, diacylglycerol; TG, triacylglycerol; Cer, ceramide; dhCer, dihydroceramide; SM, sphingomyelin; dhSM, dihydrosphingomyelin; MhCer, monohexosylceramide; Sulf, sulfatides; LacCer, lactosylceramide; GM3, monosialodihexosylganglioside; PA, phosphatidic acid; PC, phosphatidylcholine; PCe, ether phosphatidylcholine; PE, phosphatidylethanolamine; PEp, plasmalogen phosphatidylethanolamine; PS, phosphatidylserine; PI, phosphatidylinositol; PG, phosphatidylglycerol; BMP, bis (monoacylglycero)phosphate; LPC, lysophosphatidylcholine; LPCe, ether lysophosphatidylcholine; LPE, lysophosphatidylethanolamine; LPI, lysophosphatidylinositol; LPS, lysophosphatidylserine; NAPS, N-acyl phosphatidylserine; NSer, N-acyl serine.

Behavioral testing

Open Field

The OF test was used to measure motor and exploratory activity, as well as anxious-like behaviors. A square arena, delimited by transparent high walls (43.2 × 43.2 × 30.5 cm) was used, associated to an infrared detection system and a computer interface (ENV-515; MedAssociates). Mice were individually placed in the center of the arena and freely explored it for 5 minutes. The central area was defined as 25% of the total arena and the time spent in the center and periphery was calculated.

Elevated Plus Maze

Anxious behavior was specifically evaluated through the EPM test, as previously described (Walf and Frye, 2007). The plus shape apparatus was elevated 72.4 cm above the floor and consisted of two opposite open arms and two enclosed arms (50.8 cm × 10.2 cm each) (ENV-560; MedAssociates). Mice were placed individually in the center of the maze and allowed to explore for 5 minutes. An infrared detection system connected to a computer interface was used to record and automatically quantify time on each arm. The test was performed under bright light (in a dim lighted room).

Fear Conditioning

The FC protocol was performed to test contextual and cued memory. Standard operant chambers (Med Associates Inc.) (22 × 19 × 12.5 cm) with a grid on the bottom where shocks were transmitted was used, except for day 3. On the first day (fear acquisition) the subject mice was placed in the arena and allowed to explore for 5 minutes. Then a tone (80 dB) was presented for 30 s and in the last second a mild shock (0.5 mA for 1 s) was given. This was repeated for 5 blocks, with an interval of 30 s between then. On the second day the subject mice was only placed in the arena and allowed to explore for 5 minutes in order to evaluate the contextual fear conditioning. On the third day the subject mice was placed in a different arena (24 × 32 × 18.5 cm) and allowed to explore for 5 minutes. Then 5 blocks of 30 s of tone and 30 s of interval were given. This allowed cued fear conditioning evaluation. For the next 5 days an extinction protocol was performed by placing the animal in the arena and giving 15 blocks of 30 s of tone followed by 30 s of interval. 30 days after the last day of extinction spontaneous recovery was evaluated. Mice were placed in the arena and allowed to explore for 5 minutes. Then 5 blocks of 30 s of tone followed by 30 s of interval were presented. Animals were video-recorded and the percentage of freezing behavior was analyzed. All stimulation procedures were done through Med-PC IV (Med Associates Inc.) software, except for the shock that was manually given.

Morris Water Maze

The MWM test was performed to assess spatial learning and reference memory as previously described (Vorhees and Williams, 2006). A circular pool (116 cm of diameter) containing tap water was used (22 ± 1°C; 25 cm of depth) and made opaque by adding titanium oxide powder (Sigma Aldrich). The pool was divided into four imaginary quadrants and a transparent escape platform (11 cm of diameter; 24 cm high), invisible to the animals (submerged 1-2 cm below the water surface), was placed in the center of one of the quadrants. The test consisted of 5 days of acquisition plus one day for reference memory assessment, and 2 days of visual cueing. In the first 5 days mice learned to find the platform, kept in a constant position. A total of 4 trials (of a maximum of 60 s) were achieved per day, and animals were placed in different starting positions everyday. Mice had to locate the hidden platform based on distant cues distributed along the testing room walls. Animals that failed to find the platform within the trial period were gently guided to the platform and an escape latency of 60 s was registered. All mice were allowed to stay in the platform for 30 s on the first 2 days and 15 s on the subsequent 3 days during the inter-trial interval. On the 6th day a probe trial was performed (for 30 s) in which the platform was removed and the entry point was set to the quadrant opposite to the target quadrant. Visual cueing, used to detect the presence of visual and/or motivational impairments, was assessed for 2 days for which the platform was made visible by the addition of a flag and changed in location for the different trials. Time spent in each quadrant and escape latency were monitored and recorded using a video-tracking system connected to a computer (Viewpoint, Champagne-au-Mont-d'Or), to be used as readouts of task performance. Testing was conducted under dim light.

Novel Object Recognition

Since rodents are naturally exploratory and prefer to explore novelty, the NOR test was performed to evaluate recognition memory as previously described (Leger et al., 2013). The test was performed in a 30 × 30 × 30 cm arena under dimmed light and consisted of 3 days of habituation (where the animals were placed in the arena for 20 minutes) and 1 day of testing. The test was divided in two stages. First, the animal was presented with two equal objects for 10 minutes (training) and in the second phase was exposed for 5 minutes to a novel object and one of the previously examined objects. We used 1-hour interval between the two phases to assess short-term memory, in which the subject returned to its original cage. Behavior was video-recorded and time spent exploring each object was posteriorly manually scored. The discrimination ratio was calculated by dividing the time spent exploring the novel object by time spent exploring both objects.

Three-chamber Social Discrimination and Three-chamber Sociability and Preference for Social Novelty

These tests were adapted from previously described protocols (Meira et al., 2018; Moy et al., 2007) and performed on a transparent rectangular arena (56 cm long x 50 cm wide x 39 cm high) divided in three equal chambers with openings that allowed access into each chamber. The tests consisted of 10-minute trials, where the subject mice were allowed to explore the arena. After this time, when the animal stopped in the center arena, the access to the other chambers was blocked with two doors to switch trials.

The social discrimination test consisted of three trials. In the first habituation trial, mice were individually placed in the center of the arena and freely explore. In the second habituation trial, two empty round wire cups (9.8 cm high, with a bottom diameter of 8 cm and several horizontal opened bars spaced 3.7 × 0.5 cm apart which allowed nose contact between the bars) were placed on the side chambers and the subject mice freely explored the arena. In the third trial, a co-housed littermate and an unfamiliar male stranger with no prior contact with the tested mouse were each placed inside one of the wire cups. The location of the stranger and the littermate mouse was systematically alternated between mice.

The sociability and preference for social novelty test consisted of four trials. The first and second trials were similar to the ones previously described. In the third trial, an unfamiliar male mice (stranger 1), which had no prior contact with the subject mice, was placed inside one of the cups to test sociability of the subject mice. In the fourth trial, a second stranger male mice (stranger 2)

was enclosed in the previously empty cup and preference for social novelty was assessed. The location of the strangers was systematically alternated between mice. Measures were taken of the amount of time spent interacting with each cup were manually scored. Social discrimination, social preference and preference for social novelty scores were calculated as the difference between the time spent exploring the cups placed on the side chambers, divided by the total time exploring both. Testing was conducted under red light.

Dendritic Arborization

To evaluate the morphological reconstruction of hippocampal CA1 and CA3 pyramidal neurons and DG granular cells, Golgi-Cox impregnation was used according to a protocol proposed by others (Gibb and Kolb, 1998), with slight modifications. Briefly, after cervical dislocation, brains were immersed in Golgi-Cox solution (1:1 solution of 5% $K_2C_{r2}O_7$ and 5% $HgCl_2$ diluted 4:10 with 5% K_2CrO_4) and stored in the dark for 14 days, with daily agitation. Brains were then transferred to a 30% sucrose solution and stored in the dark at 4°C for at least 5 days. Coronal sections (200 μm) were obtained using a vibratome and mounted in slides that were submerged in a 28% ammonia solution, developed and fixed using Kodak Fixer (Sigma Aldrich), dehydrated and subsequently embedded in a solution containing absolute ethanol (1:3), chloroform (1:3) and xylene (1:3). Finally, samples were cleared in xylene, mounted and coverslipped. Neuronal three-dimensional reconstructions were achieved at 600x magnification using a motorized microscope (BX51, Olympus), attached to a camera (MicroBrightField Bioscience), and Neurolucida software (MicroBrightField Bioscience). 5-6 neurons were analyzed per sub-region and for each animal. The three-dimensional evaluation of the reconstructed neurons was performed using NeuroExplorer software (MicroBrightField Bioscience), and the parameters assessed included total dendritic length, total number of nodes and spine density (total spines divided by dendritic length).

Electrophysiology

Electrophysiological recordings were performed as described elsewhere (Pinto et al., 2015). The animals were anesthetized by intraperitoneal injection of Na^+-pentobarbital (40mg/kg) and decapitated. The brain was rapidly removed and placed in ice-cold sucrose-based solution containing the following (in mM): 2.5 KCl, 7 $MgCl_2$, 1.25 NaH_2PO_4, 110 sucrose, 26 $NaHCO_3$, 10 glucose, bubbled with carbogen gas (95% O_2, 5% CO_2). Slices (300 μm) transverse to the axis of the hippocampus were cut using a tissue slicer (Leica VT 1200s) and placed in a container with artificial cerebrospinal fluid (ACSF) containing (in mM): 124 NaCl, 2.5 KCl, 1 $MgSO_4$, 2 $CaCl_2$, 1.25 NaH_2PO_4, 26 $NaHCO_3$, 10 glucose, bubbled with carbogen gas and maintained at 33°C for 30 minutes. Slices were then stored at room temperature for a minimum of 30 minutes before recording. Extracellular recordings were performed in a submerge-type chamber bathed with ACSF at 31°C. A custom-made bipolar tungsten stimulation electrode was placed in the transition between CA1 and CA3, at the Schaffer collaterals, and a recording borosilicate glass pipette filled with ACSF (3-5 MΩ) was positioned in the middle of the stratum radiatum of CA1 at a predetermined fixed distance of approximately 1mm apart the stimulation electrode. Recordings were digitized with a Multiclamp 700B amplifier (Axon Instruments). Signals were low-pass filtered at 3 kHz and sampled at 10 kHz. Stimulation strength was adjusted to 30%–50% of the maximum field excitatory post synaptic potential (fEPSP) slope, after a fixed protocol of 4 increasing stimulus (2000-8000mV) was applied (input-output relationship). Before baseline acquisition, a series of paired pulse stimuli of varying interpulse interval (25, 50, 100 and 300ms) were given. The paired pulse (PP) ratio was calculated by dividing the slope of fEPSP2 by fEPSP1. A minimum of 10 minute stable baseline recordings were acquired at 0.03 Hz. LTD was elicited by delivering a low-frequency stimulation protocol consisting of 15 min 1 Hz stimulation. LTP was elicited by delivering 3 θ-burst stimuli (θ-burst: 100 Hz burst of four pulses repeated at 5 Hz with each tetanus including 10-burst trains) separated by 15 s intervals. All stored curves were an average of four consecutive recordings. Maximum EPSP slopes were calculated offline using the WinLTP software. For LTP and LTD analysis, all individual slopes were normalized to the average slope of baseline recordings. Averages of the slopes of the last 4 min recordings were used for comparison in LTP and LTD.

Gene expression analysis by qRT-PCR

Total RNA was extracted from the hippocampus using TRIzol reagent (Life Technologies, Thermo Fisher Scientific) according to the manufacturer's instructions. Then, after quantification in the NanoDrop (Thermo Fisher Scientific), 500 ng of total RNA from each sample was reverse transcribed into cDNA using the iScript cDNA Synthesis Kit (Bio-Rad) following the manufacturer's instructions. Primers used to measure the expression levels of selected mRNA transcripts by qRT-PCR were designed using the Primer-BLAST tool of the National Center for Biotechnology Information (Bethesda, MD) on the basis of the respective GenBank accession numbers. Primer DNA sequences are provided in STAR Methods. qRT-PCR was performed on a 7500 Real-Time PCR system thermocycler (Applied biosystems) and quantifications were performed in a Fast Real-Time PCR software (Applied Biosystems), with the commercial kit HOT FIREPol EvaGreen qPCR Mix Plus (ROX) (Solis Biodyne), according to the manufacturer's instructions, using equal amounts of cDNA from each sample. The cycling parameters were 1 cycle at 95°C, for 1 min, followed by 40 cycles at 95°C for 15 s, annealing temperature (primer specific) for 20 s and 72°C for 20 s, finishing with 1 cycle at 65°C to 95°C for 5 s (melting curve). Product fluorescence was detected at the end of the elongation cycle. All melting curves exhibited a single sharp peak at the expected temperature. Heat Shock Protein 90 alpha family class B member 1 (*Hsp90ab1*) was used as reference gene.

QUANTIFICATION AND STATISTICAL ANALYSIS

Western blot analysis was performed using ImageJ (NIH). The statistical analysis was performed using GraphPad Prism 7.00 software. Statistical significance was assessed by one-way ANOVA, two-way ANOVA and Student's t test, and referenced in figure legends whenever used. Values were accepted as significant when $p < 0.05$. *$p < 0.05$, **$p < 0.01$, ***$p < 0.001$. Number of mice for all statistical analyses is indicated in each legend. Values are expressed as mean ± SEM.

DATA AND CODE AVAILABILITY

This study did not generate any unique datasets or code.